AGU PUBLICATIONS

JGR

Journal of Geophysical Research: Earth Surface

RESEARCH ARTICLE
10.1002/2014JF003302

Key Points:
- Normalized distributions of shear stress are similar among sites
- Even at high flows, the bed load transport is limited to small areas of the bed
- Based on the scaling properties, a basin sediment transport model was formulated

Correspondence to:
C. Segura,
catalina.segura@oregonstate.edu

Citation:
Segura, C., and J. Pitlick (2015), Coupling fluvial-hydraulic models to predict gravel transport in spatially variable flows, *J. Geophys. Res. Earth Surf.*, *120*, doi:10.1002/2014JF003302.

Received 4 AUG 2014
Accepted 6 APR 2015
Accepted article online 14 APR 2015

Coupling fluvial-hydraulic models to predict gravel transport in spatially variable flows

Catalina Segura[1] and John Pitlick[2]

[1]Department of Forestry Engineering, Resources, and Management, Oregon State University, Corvallis, Oregon, USA, [2]Department of Geography, University of Colorado Boulder, Boulder, Colorado, USA

Abstract This study investigated spatial-temporal variations of shear stress and bed load transport at three gravel bed river reaches of the Williams Fork River, Colorado. A two-dimensional flow model was used to compute spatial distributions of shear stress (τ) for four discharge levels between one third of bankfull (Q_{bf}) and Q_{bf}. Results indicate that mean τ values are highly variable among sites. However, the properties of the mean-normalized distributions of τ are similar across sites for all flows. The distributions of τ are then used with a transport function to compute bed load transport rates of individual grain size fractions. Probability distributions of the instantaneous unit-width transport rates, q_b, indicate that most of the bed load is transported through small portions of the bed with high τ. The mean-normalized probability distributions of q_b are different among sites for all flows except at Q_{bf}, when the distributions overlap. We also find that the grain size distribution (GSD) of the bed load adjusts with discharge to resemble the grain size distribution of the subsurface at Q_{bf}. We extend these results to 13 locations in the basin, using the mean-normalized distributions of shear stress and measured subsurface grain sizes to compute bed load transport rates at Q_{bf}. We found a remarkably similar shape of the q_b distribution among sites highlighting the basin-wide balance between flow forces and GSD at Q_{bf} and the potential to predict sediment flux at the watershed scale.

1. Introduction

Natural channels are characterized by lateral and longitudinal variations in bed topography that strongly influence the distribution of fluid stresses causing sediment transport. In gravel and cobble bed channels there is generally an association between the local stresses and the grain sizes present on the bed surface, but results from a number of field and laboratory studies of transport in channels with freely formed topography show that in some cases the stresses and grain sizes are not highly correlated [*Whiting and Dietrich*, 1991; *Lisle et al.*, 2000; *Nelson et al.*, 2011]. One consequence of the mismatch between shear stress and grain size is to produce localized zones within the channel where instantaneous bed load transport rates are much higher or lower than the reach average. Thus, there can simultaneously be locations within the channel where the bed is essentially immobile and other areas where the bed material is actively being entrained and transported. These patterns are evident in measurements of bed load transport [*Emmett*, 1980; *Pitlick*, 1988; *Wathen et al.*, 1995; *Habersack and Laronne*, 2001; *Hassan and Church*, 2001; *Bunte et al.*, 2004; *Clayton and Pitlick*, 2007], displacement lengths of tracer particles [*Church and Hassan*, 1992; *Ferguson and Wathen*, 1998; *Pyrce and Ashmore*, 2003; *Yager et al.*, 2012], and scour depths associated with high flows [*Haschenburger*, 1999; *May et al.*, 2009].

Within the last 20 years there have been significant advances in the development of multidimensional hydrodynamic models, which make it possible to simulate the fluid forces governing sediment transport in high detail. Reach-scale models capable of simulating two- and three-dimensional (2-D and 3-D) patterns of velocity and shear stress have been used to examine a wide range of phenomena, including (i) details of flow patterns in river confluences and bifurcations [*Lane et al.*, 1999; *Sloff and Mosselman*, 2012] and meander bends [*Ferguson et al.*, 2003; *Legleiter et al.*, 2011]; (ii) variations in shear stress and bed mobility in single-thread channels [*Lisle et al.*, 2000; *Clayton and Pitlick*, 2007; *May et al.*, 2009; *Nelson et al.*, 2010; *McKean and Tonina*, 2013] and braided rivers [*Nicholas*, 2003; *Williams et al.*, 2013]; (iii) the influence of flow variations on in-channel habitats used by freshwater fish [*Stewart et al.*, 2005; *McDonald et al.*, 2010; *Harrison et al.*, 2011; *Papanicolaou et al.*, 2011; *Cienciala and Hassan*, 2013], migratory birds [*Kinzel et al.*, 2009], and benthic organisms [*Segura et al.*, 2011]; and (iv) the effectiveness of environmental flow releases and river restoration efforts [*Pasternack et al.*, 2004; *May et al.*, 2009; *Shafroth et al.*, 2010; *Logan et al.*, 2011].

The capabilities of 2-D and 3-D hydrodynamic models have advanced to the point where they can, in some cases, be used to predict the morphologic evolution of alluvial channels in response to changes in water and sediment supply. There are, however, several challenges in coupling flow models to transport models, particularly in channels with time-varying boundary conditions, e.g., mobile banks. Lesser but still important issues are associated with the fate of sediment moving over a bed surface that varies in texture and slopes in both the streamwise and transverse directions. Variations in texture influence the mobility of particles that are finer or coarser than the local grain size, while transverse bed slopes introduce a gravitational component to motion, such that particle trajectories are not the same as the stresses causing transport [*Engelund*, 1974]. Morphodynamic models formulated for the purpose of predicting channel evolution take many of these factors into account [*Parker and Andrews*, 1985; *Nelson*, 1990; *Mosselman*, 1998; *Sloff and Mosselman*, 2012; *Asahi et al.*, 2013; *Eke et al.*, 2014]; however, there is considerable uncertainty in the parameterization of functions that account for the influence of variations in grain size and bed topography on sediment transport.

Our main objective in this paper is to develop a simplified yet physically based model of bed load transport in channels with spatially variable flow fields. We use a two-dimensional hydrodynamic model to parameterize spatial distributions of shear stress at four different discharges in three separate reaches of a gravel bed river. We assume that within each reach, every part of the bed experiencing the same level of shear stress above the threshold for motion will transport the same amount of bed load. For each discharge, we divide the model-derived estimates of shear stress for the reach into a series of intervals and for each interval compute the bed load transport rate using a subsurface-based transport relation. The individual transport rates are weighted by the proportion of the bed experiencing that shear stress then summed to estimate the total load for that flow. Finally, we formulate a watershed-scale model based on a collapse of the shear stress distributions at the three study sites to predict bankfull bed load transport rates at 13 other sites where we have measurements of channel geometry and subsurface grain size distributions (GSD). We show that the shapes of the normalized distributions of bankfull bed load are approximately the same from one reach to another highlighting a basin-wide balance between flow forces and GSD.

2. Study Area

This investigation was conducted in three gravel bed alluvial reaches of the Williams Fork River, Colorado. The relatively undisturbed mountain catchment has a stream network with two main tributaries that join about one third of the way downstream into a single-thread river that drains into the Williams Fork Reservoir (Figure 1). The drainage area above that point is about 385 km^2. The Williams Fork basin is underlain by Precambrian metamorphic and igneous rocks that were uplifted as part of the Williams Range thrust of the Laramide orogeny [*Tweto and Reed*, 1973]. Sites 1 and 2 are located in relatively narrow valleys of the South Fork and North Fork, whereas Site 3, in the main stem, is located in a very wide valley. Sites 1 and 2 are underlain by till glacial outwash [*Kellogg*, 2001], and Site 3 is underlain by alluvium including terrace gravels [*Tweto and Reed*, 1973]. The study sites are located in straight to mildly sinuous reaches in the vicinity of gaging stations operated by the U.S. Geological Survey (USGS). The sites display weakly developed pool-riffle morphologies and are bordered by prominent floodplains with limited bank erosion. Channel properties including reach-averaged slope, bankfull width, depth, bed material grain size, and bankfull discharge (Q_{bf}) are presented in Table 1. Q_{bf} varies between 7.0 and 20.1 m^3/s for the three sites (Table 1). Elevations within the basin range from 2380 m at the Williams Fork Reservoir to about 4000 m at the Continental Divide near the west side of Berthoud Pass (Figure 1). The basin is located in the Arapahoe National Forest dominated by tree species such as engelmann spruce (*Picea engelmannii*), subalpine fir (*Abies lasiocarpa*), and lodgepole pine (*Pinus contorta*). Most of the annual precipitation is received as snow during the winter months [*Serreze et al.*, 1999]. The discharge regime of the river is typical of snowmelt-dominated systems, with the annual peak flow occurring in mid-June [*Segura and Pitlick*, 2010; *Segura et al.*, 2011].

3. Methods

3.1. Field Methods

Detailed measurements of channel geometry, bed material grain size, and flow properties were taken in three alluvial reaches located on the South Fork, North Fork, and main stem of the Williams Fork River, respectively.

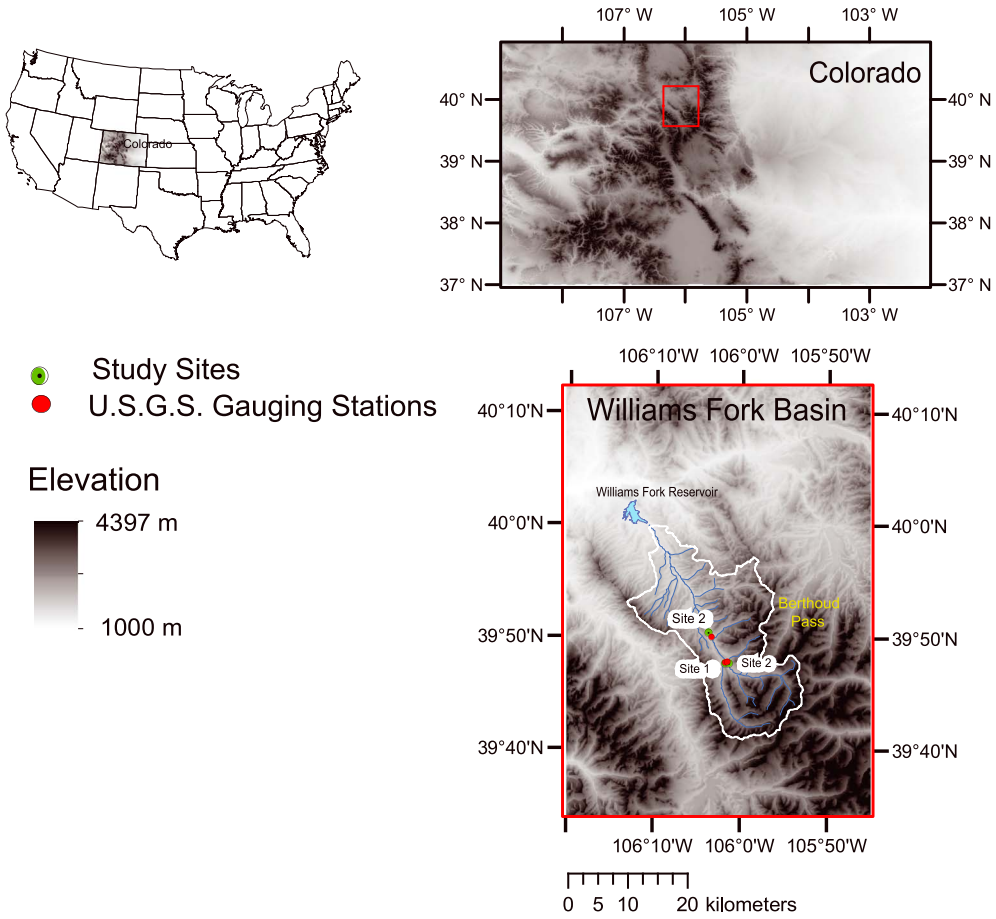

Figure 1. Location of the Williams Fork drainage basin in Colorado.

At each site, we surveyed between 13 and 18 cross sections spaced roughly a half-channel width apart. These measurements were used to develop maps of the bed topography (Figure 2), which were then used as input to the flow model. Samples of the bed material were taken in each reach to characterize the GSD of the surface and subsurface sediment (Table 1 and Figure 3). Bed surface grain sizes were determined from point counts totaling 2500, 2750, and 4750 particles at Sites 1, 2, and 3, respectively. Bulk samples of the subsurface sediment were taken from exposed bars after removing the surface layer; total sample weights range between 38 and 270 kg and were large enough to ensure that the largest grain in the sample was

Table 1. Characteristics of the Three Study Sites

Characteristic	Site 1	Site 2	Site 3
Location (Figure 1)	South Fork	Middle Fork	Main Stem
USGS gage no.	09035900	09035700	09036000
Elevation (m)	2730	2730	2660
Drainage area (km^2)	70.7	90.6	231
Slope, S (m/m)	0.0155	0.0049	0.0039
Bankfull width, B (m)	10.5	11.7	25.2
Bankfull depth, H (m)	0.58	0.54	0.63
Bankfull hydraulic radius, R (m)	0.54	0.55	0.6
Bankfull discharge (m^3/s)	7	10.5	20.1
D_{50} (mm) ± standard error	71 ± 7	61 ± 2	40 ± 1
D_{84} (mm) ± standard error	134 ± 11	105 ± 2	73.5 ± 2
D_{50s} (mm)	24	14	10

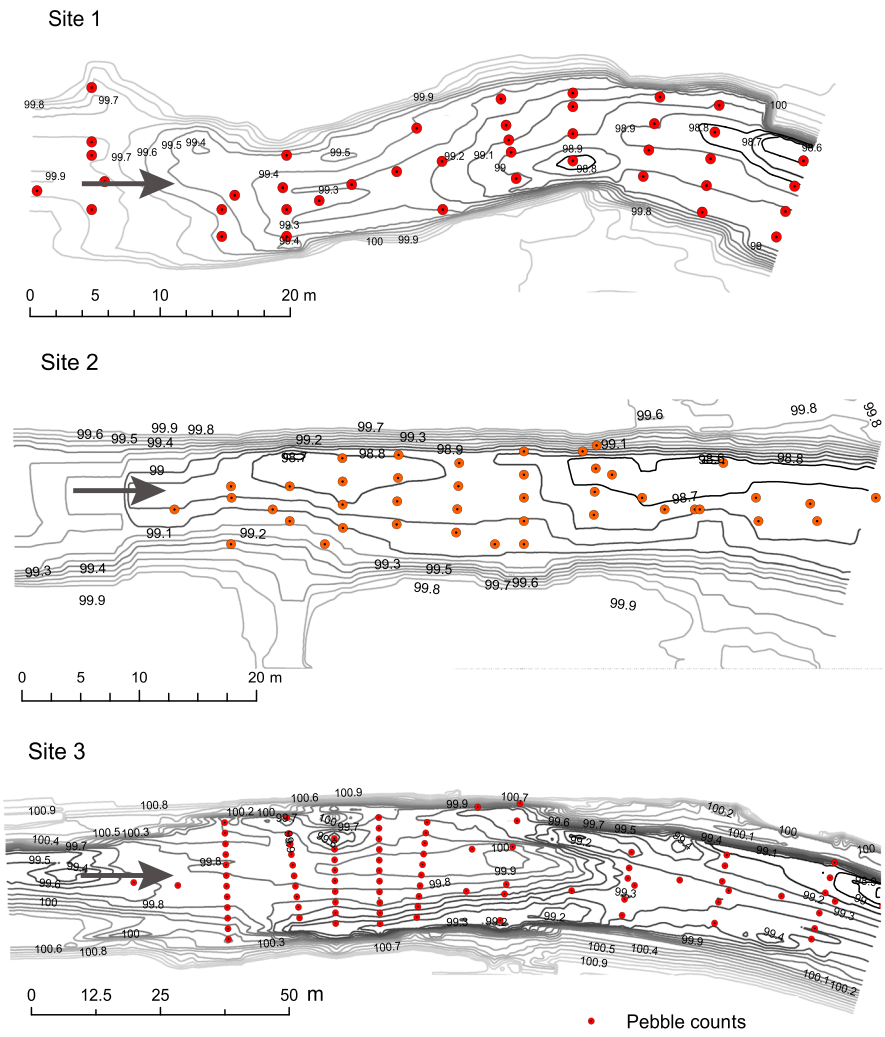

Figure 2. Topography and pebble counts sampling locations of the study sites. Contour lines are every 10 cm with respect to an arbitrary datum of 100 m.

no more than 5% of the total weight [*Church et al.*, 1987]. Finally, we also measured water surface elevation (WSE) and velocity at four different flows per site ranging from one third to full Q_{bf} conditions.

3.2. Flow Model

Estimates of the local velocity and shear stress were obtained using the two-dimensional hydrodynamic and sediment transport model FaSTMECH under the MD-SWMS interface (now iRIC system) developed by the U.S. Geological Survey [*McDonald et al.*, 2001, 2006]. This model computes the downstream and cross-stream components of velocity (u and v, respectively) using a finite difference solution to the Reynolds-averaged momentum equations [*Nelson et al.*, 2003]. The equations are cast in an orthogonal curvilinear coordinate system that follows the channel planform trace [*Nelson and Smith*, 1989]. The input data for the model are detailed topography, discharge, WSE at the downstream end, and bed roughness, expressed as a roughness length or drag coefficient [*Lisle et al.*, 2000]. The grid over which the values of velocity and shear stress were computed at each site had a resolution of ~1 m with the number of nodes varying between 1021 and 5898 (Table 2). The lowest flow modeled at each site corresponds roughly to the threshold for motion for streams in this setting [*Torizzo and Pitlick*, 2004], and the highest flow corresponds to Q_{bf}. Calibrations of the model were based on observations of WSE taken at a minimum of 15 points along the margins of each reach and measurements of mean flow velocity taken at flows that were safe to wade.

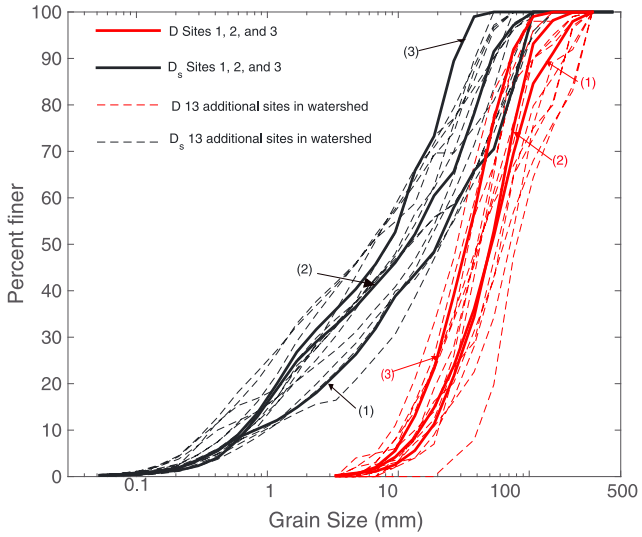

Figure 3. Grain size distributions of surface, D, (red lines) and subsurface, D_s, (black lines) at the three study sites (solid lines) and 13 additional locations in the watershed (dashed lines).

The FaSTMECH model calculates shear stress (τ) in the downstream (x) and cross-stream (y) directions based on the two components of velocity, u and v, respectively, and an estimate of channel roughness:

$$\tau_x = \rho C_d u \sqrt{(u^2 + v^2)} \quad (1a)$$

$$\tau_y = \rho C_d v \sqrt{(u^2 + v^2)} \quad (1b)$$

where ρ is the density of water and C_d is a dimensionless drag coefficient. The model can handle spatial variations in roughness and bed grain size using two different approximations. In the simplest case, one can assume that the flow averages the roughness over the reach, and therefore, the drag coefficient is set to a constant, which can be adjusted to improve the agreement between the observed and predicted values of the WSE and velocity. Alternatively, one can assume that the flow responds instantaneously to variations in grain size, and therefore, the drag coefficient mirrors the local GSD. In this case the roughness is computed based on the local grain size derived from pebble count measurements (Figure 2), and the depth and drag coefficients are adjusted locally to improve the agreement between model results and observations. The choice of either constant or variable roughness depends on the heterogeneity of the bed sediment. Both alternatives were explored in this study for all flows modeled. In addition, the lateral eddy viscosity (LEV), which is a measure of momentum transfer in the cross-stream direction, can be adjusted in the model to obtain better agreement between observed and predicted values of WSE and mean velocity, $\bar{U}$.

The model was calibrated for a series of flows by adjusting the drag coefficient (C_d) and lateral eddy viscosity (LEV) to minimize the root-mean-square difference between predicted and measured values of WSE and $\bar{U}$.

Table 2. Characteristics of the Modeled Flows per Site and Modeling Results: Flow Size (Q_i), Ratio of Q_i to Bankfull Flow (Q_{bf}), Mean Model Flow Depth (H_{mean}), Hydraulic Radius (R) Derived From Field Observations, Root-Mean-Square (RMS) of the Difference Between Observed and Modeled Values of Water Surface Elevation (WSE) and Mean Vertical Velocity ($\bar{U}$), Coefficient of Determination (R^2) of the Relation Between Observed and Predicted WSE and $\bar{U}$, 1-D Field-Based Shear Stress Estimate ($\tau = \rho g R S$), Modeled Mean, Median, and Maximum Shear Stress (τ), Ratio of the Mean-Modeled Flow Depth to D_{84}, and Percentage of Channel Bed With Shields Stress for the Median Surface Grain Size Above Critical for Motion $(\tau_{50}^* > \tau_c^*)$

Site	Q_i (m^3/s)	Q_i/Q_{bf}	# Nodes	H_{mean}	R (m)	RMS-WSE (m)	RMS-$\bar{U}$ (m/s)[a]	R^2 WSE	R^2 $\bar{U}$	$\tau_{(1\text{-d})}$ (N/m^2)	τ_{mean} (N/m^2)	τ_{median} (N/m^2)	τ_{max} (N/m^2)	H/D_{84}	% of Bed $\tau_{50}^* > \tau_c^*$
1	1.9	0.27	1021	0.29	0.28	0.050	0.24	0.99	0.87	42.6	31.6	30.7	87.12	2.16	7.12
1	3.1	0.44	1069	0.37	0.35	0.037	0.28	0.99	0.70	53.2	42.5	43.8	94.71	2.76	16.4
1	5.5	0.79	1136	0.47	0.44	0.050	NA	0.99	NA	66.9	58.7	62.3	118.1	3.51	49.0
1	7[b]	1.0	1174	0.58	0.54	0.046	NA	0.99	NA	82.1	63.1	66.3	130.7	4.33	54.3
2	2.9	0.28	1727	0.35	0.35	0.023	0.17	1.00	0.75	16.6	11.8	11.5	44.61	3.33	0.91
2	4.9	0.47	1866	0.42	0.42	0.021	0.10	0.98	0.90	20.2	16.2	16.9	41.72	4.01	5.9
2	8.1	0.77	2056	0.52	0.52	0.026	NA	0.99	NA	25.0	20.8	22.8	49.0	4.95	13.3
2	10.5[b]	1.0	2124	0.55	0.55	0.033	NA	0.98	NA	26.4	23.1	26.0	52.72	5.24	24.7
3	6.2	0.31	4220	0.36	0.36	0.023	0.21	1.00	0.97	13.8	10.6	10.5	35.63	4.92	8.42
3	9.1	0.45	4642	0.43	0.42	0.032	0.14	0.99	0.99	16.1	13.1	13.3	34.81	5.85	18.6
3	15.9	0.79	5555	0.59	0.57	0.025	NA	0.99	NA	21.8	17.4	18.1	34.62	8.03	44.2
3	20.1	1.0	5898	0.63	0.60	0.032	NA	0.99	NA	23.0	21.0	22.6	41.42	8.57	65.3

[a]Mean vertical velocity represented by measurements of flow velocity at 0.6 times the depth from the water surface. Velocity measurements were possible at flows below $0.5Q_{bf}$ for all sites. Velocity was measured at cross sections 6 and 10 for Site 1; 2 and 3 for Site 2; and 2, 4, and 6 for Site 3.
[b]Even though these flow conditions were not observed in Sites 1 and 2, a model run was possible based on observations of bankfull flow level.

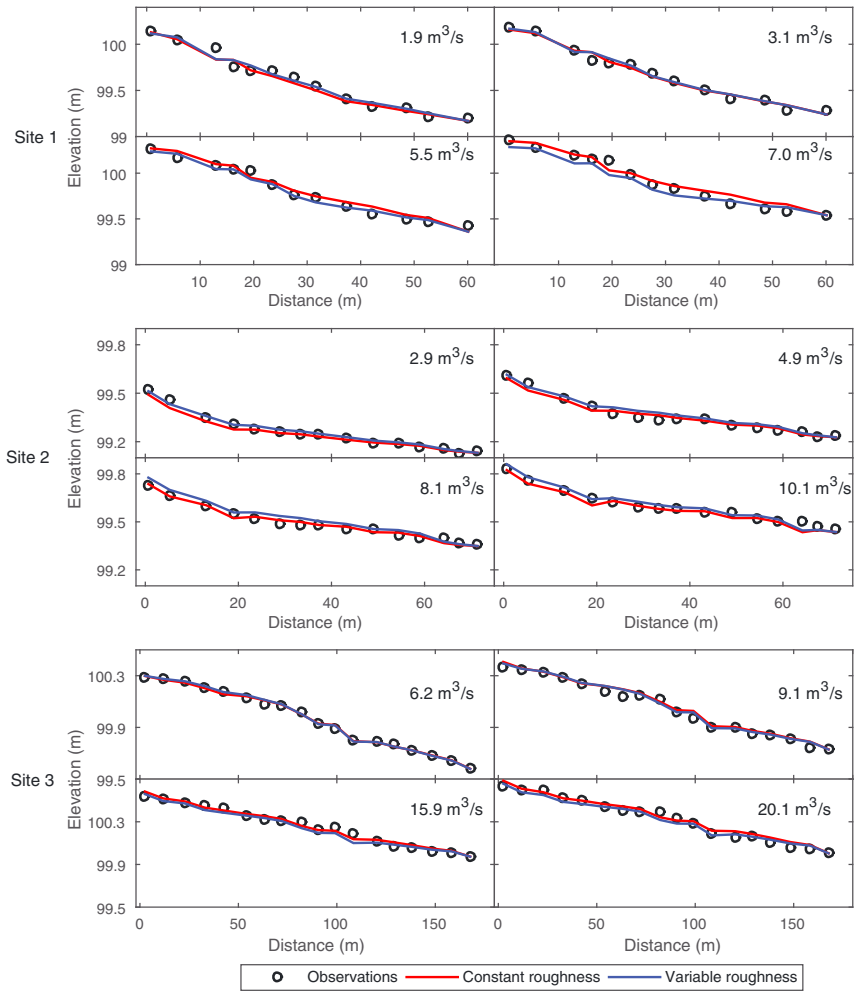

Figure 4. Comparison of modeled and observed water surface elevations (WSE) for four flows at Sites 1–3. Each panel presents predicted WSE assuming both constant and variable roughness.

The best results were obtained using a constant roughness, with C_d values ranging between 0.012 and 0.050 and LEV values ranging between 0.002 and 0.05 m^2/s; results obtained with variable roughness were nearly the same with LEV values ranging between 0.002 and 0.08 m^2/s. All runs were performed with the default relaxation coefficients. The results, presented in Figures 4 and 5 and Table 2, indicate that in most cases the agreement between predicted and measured values of WSE and $\bar{U}$ was quite strong, regardless of whether the roughness was treated as constant or variable. The root-mean-square (RMS) difference between predicted and measured values varied between 0.021 and 0.05 m for WSE and between 0.10 and 0.28 m/s for $\bar{U}$ (Table 2). The agreement between predicted and measured values of WSE was strong for all the 12 flows modeled ($R^2 > 0.97$, Table 2). For $\bar{U}$ the agreement between observed and predicted values yielded strong fits ($R^2 > 0.87$, Table 2) in four out of the six flows for which velocity measurements were taken. In the remaining two flows the agreement was weaker ($R^2 > 0.75$, Table 2) likely because, in these two cases, high relative roughness (ratio of grain size to flow depth) contributed to higher discrepancies. The results presented in Figures 4 and 5 also show that the effects of varying the drag coefficient, C_d, or setting it as a constant are small. The RMS difference between predicted and measured WSE and velocity varied between 0.016 and 0.059 m and between 0.07 and 0.25 m/s, respectively, for predictions based on variable C_d. These differences are similar to those obtained with a constant roughness assumption (Table 2) suggesting that model-derived estimates of shear stress and velocity are not especially sensitive to variations in the bed surface GSD. In addition, a comparison between the distribution of the median surface grain size, D_{50}, and

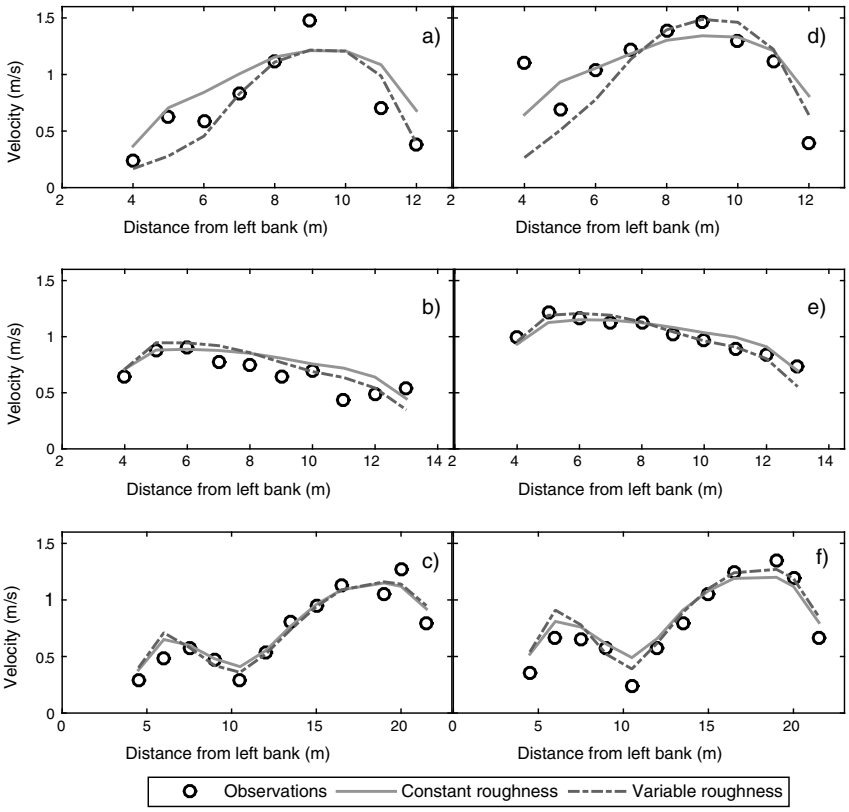

Figure 5. Comparison of model-generated vertically mean flow velocity ($\bar{U}$) and measured velocity at 0.6 times the depth from the water surface in a cross section of each study site for two flows: (a and d) cross section 6 at Site 1 for flows of 1.9 and 3.1 m^3/s, (b and e) cross section 2 at Site 2 for flows of 2.9 and 4.9 m^3/s, and (c and f) cross section 6 at Site 3 for flows of 6.2 and 9.1 m^3/s. Each panel presents predicted $\bar{U}$ assuming both constant and variable roughness.

the distribution of shear stress at different flows indicated that the variability in D_{50} is much smaller than the variability in shear stress. The coefficient of variation of the shear stress in all runs ranges from 47% to 61%, whereas the coefficient of variation of the D_{50} ranges from 11 to 36% [*Segura et al.*, 2011]. Therefore, the simpler solution of spatially constant roughness and bed surface grain size was assumed for all model runs.

We compared model-derived estimates of the mean shear stress with the reach-averaged shear stress:

$$\tau = \rho g R S \tag{2}$$

where g is the gravitational acceleration, R is hydraulic radius obtained from channel geometry measurements, and S is water surface slope. Equation (2) is also used as part of the strategy for scaling results from the three study sites to other locations in the watershed (see section 4.3).

3.3. Bed Load Transport

Transport rates for individual grain size fractions of the subsurface sediment were calculated for each modeled flow using the subsurface-based transport relation of *Parker and Klingeman* [1982]. The rationale for computing transport rates with respect to the subsurface sediment is that this sediment includes the sand sizes which are commonly found in the bed load [*Lisle*, 1995; *Hassan and Church*, 2001; *Mueller et al.*, 2005; *Clayton and Pitlick*, 2007; *Recking*, 2010], but not on the bed surface. We computed transport rates for each size fraction based on the distributions of shear stress estimated from the flow model and the relative abundance of subsurface grain sizes likely to move as bed load. Fractional transport rates were then weighted by the proportion of the bed experiencing a given shear stress, and those values were summed to get the total bed load.

The transport relation presented by *Parker and Klingeman* [1982] is based on *Parker*'s [1979] approximation of the Einstein bed load function

$$G = 5.6\times10^3\left(1-\frac{0.853}{\phi}\right)^{4.5} \tag{3}$$

where the parameters G and ϕ are, respectively,

$$G = \frac{W^*}{W_r^*} \tag{4}$$

and

$$\phi = \tau^*/\tau_r^*. \tag{5}$$

In these equations, W^* is a dimensionless transport rate, τ^* is a dimensionless shear stress, and the subscript r refers to reference values of W^* and τ^*associated with a small but measureable transport rate. These two dimensionless parameters are defined as follows:

$$W^* = \frac{(s-1)gq_b}{(\tau/\rho)^{1.5}} \tag{6}$$

and

$$\tau^* = \frac{\tau}{(\rho_s-\rho)gD} \tag{7}$$

where s is the specific gravity of sediment, q_b is the volumetric transport rate per unit width of channel, τ is the bed shear stress, ρ_s is the density of sediment, and D is the grain size.

Equation (3) was initially formulated for uniform grain sizes and transport stages greater than 1.0; however, the equation can be modified for mixtures and low transport rates using several additional assumptions and relations. First, we write (3) in a more familiar way by assuming a reference transport rate of $W_r^* = 0.002$ [*Parker et al*., 1982; *Wilcock*, 1988]. Second, we add another function that produces finite transport rates for low transport stages, $\phi \leq 0.853$ [*Parker*, 1990; *Wilcock*, 2001]. Last, we modify the transport functions to compute transport rates for individual size fractions i of the subsurface sediment. This results in a two-part transport relation applicable to a mixture of sizes:

$$W_i^* = 11.2\left(1-\frac{0.853}{\phi_i}\right)^{4.5} \quad \text{for} \quad \phi > 0.853 \tag{8a}$$

and

$$W^* = 0.0025\phi_i^{14.2} \quad \text{for} \quad \phi \leq 0.853 \tag{8b}$$

The mobility of individual sizes is determined with a hiding function

$$\phi_i = \frac{\tau_{r,is}^*}{\tau_{r,50s}^*} = \left(\frac{D_{is}}{D_{50s}}\right)^{-b} \tag{9}$$

where $\tau_{r,is}^*$ is the reference shear stress for an individual grain size, D_{is}, $\tau_{r,50s}^*$ is the reference shear stress for the median grain size of the subsurface, D_{50s}, and b is an exponent reflecting the extent to which transport is size selective; we set $b = 0.982$ [*Parker et al*., 1982].

We estimated $\tau_{r,50s}^*$ assuming that it scales with the reference Shields stress for the median surface grain size, $\tau_{r,50}^*$, and the ratio of the surface to subsurface median grain sizes:

$$\tau_{r,50s}^* = \tau_{r,50}^*\left(\frac{D_{50}}{D_{50s}}\right) \tag{10}$$

$\tau_{r,50}^*$ was determined for each of the three study sites using the reference Shields stress relation presented by *Mueller et al*. [2005]:

$$\tau_{r,50}^* = 0.021 + 21.8S \tag{11}$$

Transport rates were calculated for each size fraction (D_i) and each increment of shear stress (τ_j), for four flow levels:

$$W_{ij}^{*} = \frac{(s-1)gq_{b,ij}}{f_{D,i}\left(\frac{\tau_j}{\rho}\right)^{1.5}} \tag{12}$$

where $q_{b,ij}$ is the unit-width transport rate for grain size i and shear stress, j, and $f_{D,i}$ is the fraction of sediment in each size class. The shear stress increments were defined from zero to the maximum observed in increments of 0.5 N/m^2. The width-integrated transport rate for a given flow, Q_b, is thus the sum of the fractional transport rates per grain size and shear stress weighted by the grain size and shear stress frequency distributions:

$$Q_b = B\rho_s \sum_i \sum_j q_{b,ij} f_{\tau,j} \tag{13}$$

where B is the channel width and $f_{\tau,j}$ is the fraction of the bed experiencing shear stress τ_j This approach assumes that the model grid cells have uniform width; for our reaches the grid width was ~1 m. The approach would need to be modified if cell widths were not equal.

The bed load calculations were performed for all grain sizes in the subsurface likely to move as bed load. Thus, small particles likely to move in suspension were excluded by assuming that significant suspension occurs if the near-bed shear velocity, u^*, exceeds the sediment settling velocity [*Bagnold*, 1966]. For each flow, u^* was calculated as

$$u^{*} = \sqrt{gHS} \tag{14}$$

where H is the flow depth. The settling velocity was calculated using an empirical equation [*Dietrich*, 1982], and the subsurface GSDs were truncated at the maximum grain size likely to be in suspension (Table 3).

3.4. Analysis of the Distributions of Shear Stress and Bed Load

Maps of the spatial distributions of shear stress (τ) and fractional bed load $\left(q_b = \sum_i q_{b,ij}\right)$, along with their mean-modeled normalized histograms, were produced to compare patterns between flows and sites. The frequency distributions of τ and q_b were fitted to a two-parameter gamma function, which has been used in previous studies to characterize the distributions of τ and H [*Paola*, 1996; *Nicholas*, 2000; *Pitlick et al.*, 2012; *Recking*, 2013]:

$$f(x) = \frac{\alpha^{\alpha}\left((x/\langle x\rangle)^{\alpha-1}e^{-\alpha(x/\langle x\rangle)}\right)}{\langle x\rangle\Gamma(\alpha)} \tag{15}$$

where Γ is the standard gamma function, α is a shape parameter, and $x/\langle x\rangle$ is the mean-normalized shear stress (or fractional bed load transport rate (q_b)). The second parameter of the gamma function (i.e., scale parameter) is equal to $\langle x\rangle/\alpha$. Normalized histograms of τ and q_b were formed by grouping values into 1000 bins of equal size that varied between 0 and 4 for $\tau/\langle\tau\rangle$ and between 0 and 45 for $q_b/\langle q_b\rangle$. These ranges included all the observations of τ and q_b in each of the 12 flows analyzed (Tables 2 and 3). The number of counts per bin was normalized by the bin width, dτ or dq_b, to produce frequency distributions where the number of observations is independent of the interval width [*Newman*, 2005; *Segura and Pitlick*, 2010]. If the number of observations in a given bin was less than five, two consecutive bins were joined to improve statistics. The normalized distributions of τ were computed for all observations, whereas the distributions of q_b were computed excluding transport rates equal to zero. By doing this, we eliminated all the areas of the channel bed where the stress appears to be lower than the threshold for motion for all grain sizes likely to move as bed load. The parameters of the gamma function that best fitted the distributions were found by systematically varying the α parameter between 0 and 60 in increments of 0.01 (i.e., total 6000 α values tested) and finding the parameter values that yielded the lowest overall χ^2 score [*Bevington and Robinson*, 2003; *Press et al.*, 2007; *Segura and Pitlick*, 2010]:

$$\chi^2 = \sum \frac{[f_k - f(x_k)]^2}{\sigma_k^2} \tag{16}$$

Table 3. Median Grain Size of the Subsurface (D_{50s}): Largest Particle Size Likely to Travel in Suspension (D_{max}), Median Grain Size of the Subsurface Excluding Particles Likely to Travel in Suspension (D_{50st}), Critical Shields Stresses for Motion of the Median Grain Size of the Surface $\left(\tau^*_{r,50}\right)$ and Subsurface Size $\left(\tau^*_{r,50s}\right)$; Median Grain Size of the Load ($D_{50,qb}$); Total Modeled Width-Integrated Bed Load Transport (q_b); and Parameters, Reduced Chi-Square $\left(\chi^2_\nu\right)$, and Root Mean Square Error (RMSE) of the Gamma Function Fitted to the Distributions of Shear Stress (τ) and q_b for Every Flow in Each Site

										Γ Parameter (τ)				Γ Parameter (q_b)			
Site	Q (m^3/s)	D_{50s} (mm)	D_{max} (mm)	D_{50st} (mm)	$\tau^*_{r,50}$ [a]	$\tau^*_{r,50s}$ [b]	$D_{50,qb}$ (mm)	q_b (kg/m/s)	% Bed With Zero q_b	α	θ	χ^2_ν	RMSE	α	θ	χ^2_ν	RMSE
1	1.9	24	1.0	28.6	0.055	0.136	5.3	0.0101	84.6	4.09	10.40	2.00	0.35	0.04	0.35	21.78	3.60
1	3.1	24	1.4	29.7	0.055	0.131	8.2	0.0489	64.4	3.26	9.70	1.52	0.31	0.08	0.74	13.02	2.45
1	5.5	24	1.4	29.7	0.055	0.131	11.1	0.4157	37.3	4.81	12.21	3.00	0.53	0.18	2.66	4.63	1.26
1	7.0	24	1.4	29.7	0.055	0.131	25.8	0.6498	32.6	4.87	12.97	0.44	0.44	0.19	4.37	4.55	1.18
2	2.9	10	0.5	15.9	0.032	0.122	1.9	0.0013	94.1	3.07	5.28	3.15	0.40	0.02	0.19	46.39	4.99
2	4.9	10	0.5	15.9	0.032	0.122	1.5	0.0042	86.4	4.21	2.80	3.69	0.42	0.04	0.12	25.79	2.87
2	8.1	10	1.0	19.1	0.032	0.101	3.7	0.0227	63.0	4.00	5.20	6.21	0.55	0.08	0.27	15.39	1.90
2	10.5	10	1.0	19.1	0.032	0.101	4.3	0.0347	48.6	4.42	5.23	7.51	0.60	0.11	0.40	10.36	1.35
3	6.2	14	0.5	11.5	0.03	0.102	3.2	0.0115	81.8	2.89	3.67	2.94	0.26	0.13	0.47	6.92	1.69
3	9.1	14	0.5	11.5	0.03	0.102	2.7	0.0153	62.2	4.73	2.77	2.94	0.28	0.14	0.28	9.05	1.05
3	15.9	14	0.5	11.5	0.03	0.102	3.0	0.0574	34.5	5.54	3.14	6.05	0.33	0.23	0.38	4.65	0.65
3	20.1	14	1.0	12.8	0.03	0.092	6.7	0.1701	13.7	5.45	3.83	7.63	0.37	0.27	0.73	4.36	0.59

[a] Computed based on slope [*Mueller et al.*, 2005].
[b] Computed based on $\tau^*_{c,50}$ (see text, equation (10)).

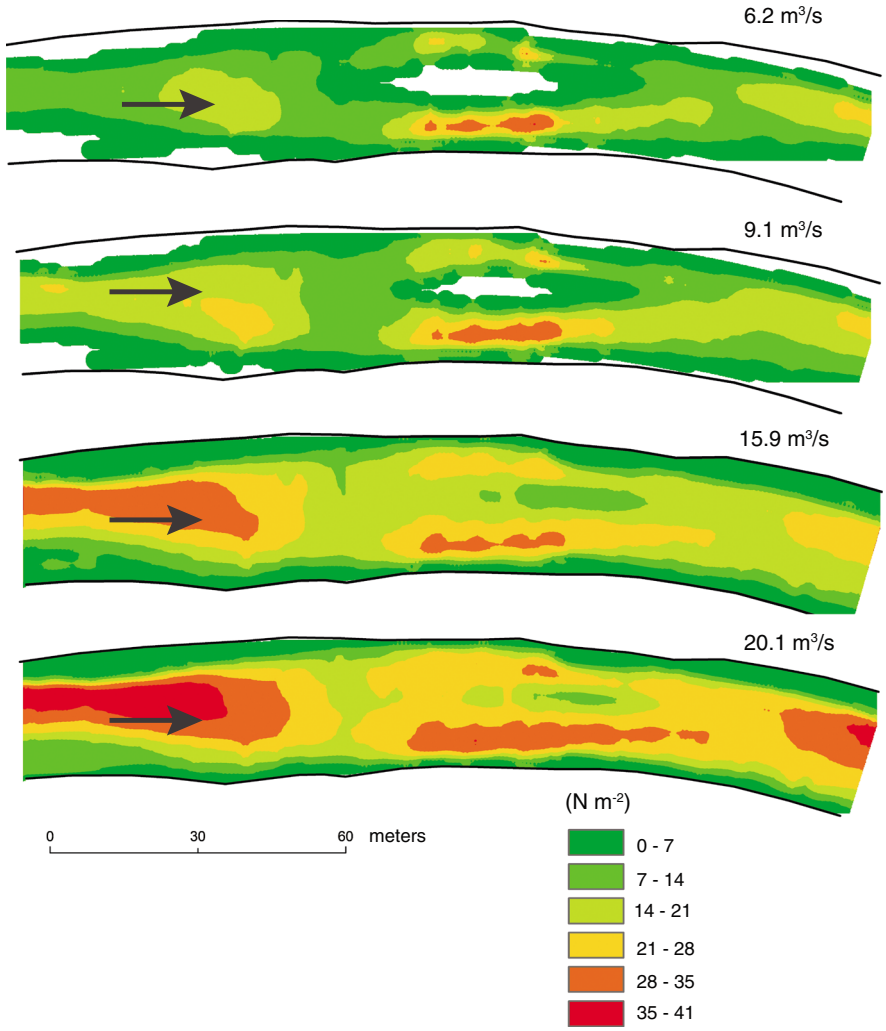

Figure 6. Model output of shear stress at Site 3 for four discharge levels between 6.2 ($0.3Q_{bf}$) and 20.1 m^3/s (Q_{bf}).

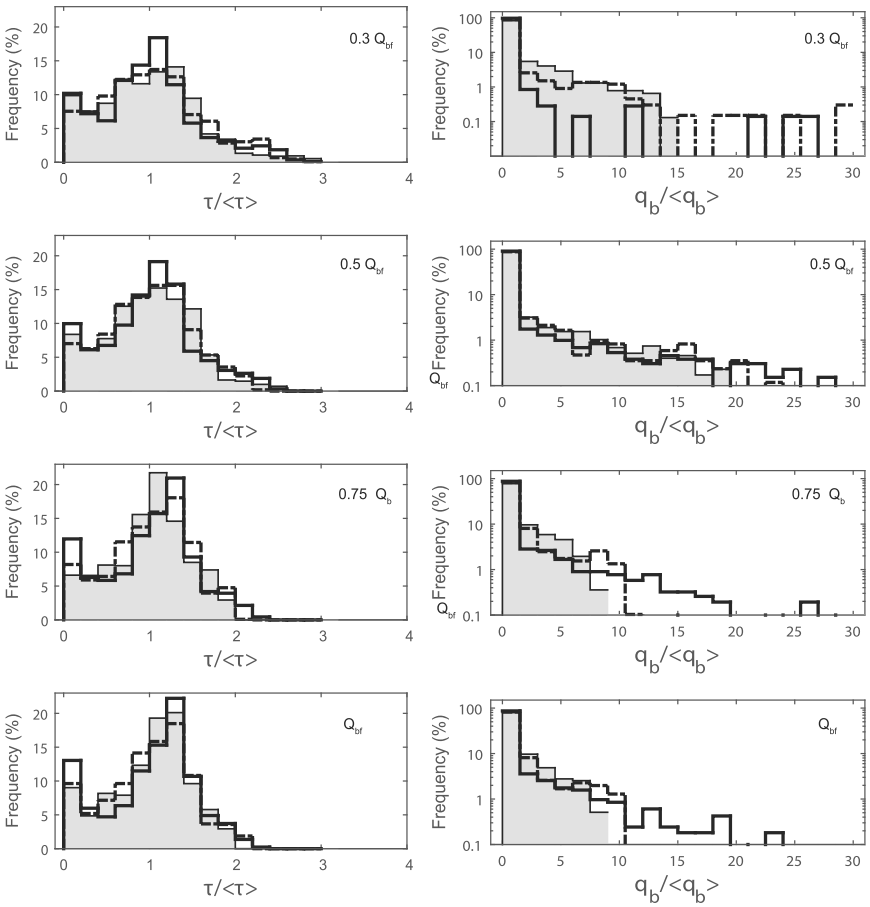

Figure 7. Frequency distribution of shear stress, τ, and instantaneous unit-width bed load, q_b, normalized by their mean, $\langle\tau\rangle$ or $\langle q_b\rangle$, for four flows at three sites. Site 1 corresponds to the dashed line, Site 2 to the solid line, and Site 3 to the gray area.

where f_k is the observed frequency of τ or q_b in a given bin interval, k, $f(x_k)$ is the predicted frequency of τ or q_b by the gamma function, and σ_k is the uncertainty associated with the observed frequencies. The uncertainty was computed as the square of the number of observations in each bin [*Bevington and Robinson*, 2003; *Press et al*., 2007]. We assessed the goodness of fit of the gamma function by computing the reduced χ^2,χ^2_ν, which is equal to the χ^2 divided by the number of degrees of freedom, and the root-mean-square error, RMSE. An excellent fit should yield $\chi^2_\nu \leq 1$ and RMSE of 0 [*Bevington and Robinson*, 2003; *Press et al*., 2007].

4. Results

4.1. Variations in Shear Stress

Table 2 summarizes the model results for each site for four flows varying between approximately one third Q_{bf} and Q_{bf}. We use Site 3 as an example to show the variability in the spatial distribution of shear stress during the four modeled flows (Figure 6). As discharge increases, the spatial distribution of τ is progressively dominated by high shear stress areas. The areas of the channel bed that experience the highest values of shear stress are partially controlled by channel topography. At Site 3, high values of shear stress were consistently observed along the right bank where the flow is constrained to a smaller area as it goes around a midchannel bar and in the pool located in the left side of the downstream end of the reach (Figure 6).

The distributions of shear stress scaled by their mean-modeled value, $\langle\tau\rangle$, were plotted for each level of discharge at all three sites (Figure 7). Although the shapes of the distributions change with flow, it appears that for a given flow the distributions are similar among the three sites. At low flows ($Q < 0.5Q_{bf}$) the distribution of τ is right skewed, with most of the bed experiencing shear stresses lower than the reach

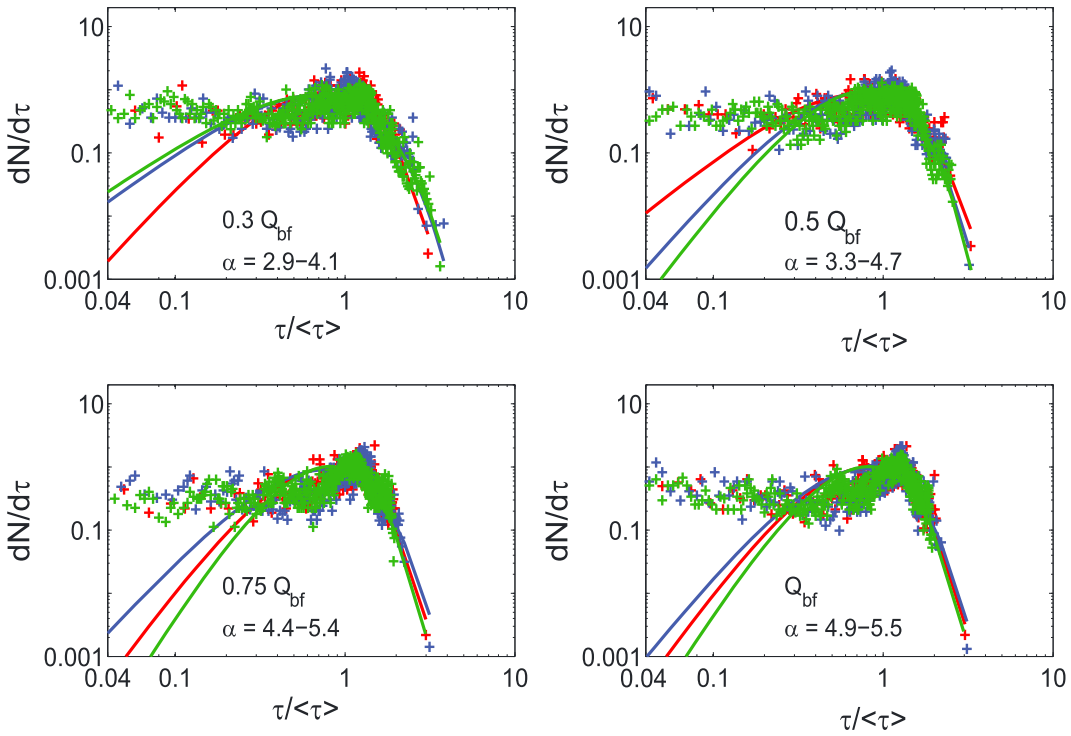

Figure 8. Frequency distributions of normalized shear stress, τ, at four discharge levels and at three sites. The colored lines in each panel indicate the best fit to the gamma function. The red markers and lines are for Site 1, blue for Site 2, and green for Site 3.

mean (Figure 7). As discharge increases, the distribution of τ becomes more symmetric, and at the highest discharges modeled (Q_{bf}) between 54 and 58% of the bed experiences $\tau > \langle\tau\rangle$. The range of the normalized shear stress distributions also changes with discharge, becoming narrower as flow increases. For flows below $0.5Q_{bf}$, the range in τ is up to 4 times $\langle\tau\rangle$, while for the highest modeled flow (Q_{bf}), the range in τ is up to 2.3 times $\langle\tau\rangle$. This change in shape arises because of the decreased effect of the bed roughness with increasing discharge and flow depth.

In order to investigate the degree of similarity among τ distributions per flow level, we computed the difference between the frequency distributions for each site and the average frequency distribution among all three sites (i.e., average of the frequency distributions of τ in each panel in Figure 7). The results of this analysis suggest that frequency differences are always below 20% for shear stress values below $2\langle\tau\rangle$, where most of the τ estimates are concentrated. This agreement implies that the distribution of shear stress for each of the four flows ($0.3Q_{bf}$, $0.4Q_{bf}$, $0.75Q_{bf}$, and Q_{bf}) can be scaled to other locations in the watershed for which $\langle\tau\rangle$ is known with a level of accuracy better than 20%. The degree of similarity among τ distributions per flow level is further emphasized based on gamma function fits to the normalized distributions of τ (Figure 8). From the results shown in Figure 8 it is evident that the gamma function captures the variability of high values of shear stress relatively well in comparison to low values, where the discrepancies are up to 2 orders of magnitude. The χ^2_v and RMSE of the fits varied between 0.44–7.6 and 0.26–0.6, respectively (Table 3). We computed both objective functions eliminating $\tau/\langle\tau\rangle$ frequencies below the 5th to the 75th percentiles and found that both decreased, meaning the fits are stronger at high shear stress values (Figure 9). For instance, the strength of the fits eliminating values below the 45th percentile improved the fits from a mean χ^2_v of 4 to 1.5 and from a mean RMSE of 0.4 to 0.3 (Figure 9). Thus, the gamma function characterizes the distribution of shear stress quite well in the range of values responsible for most of the bed load transport. In addition, we find that the shape parameter (α) is similar across sites at individual flow levels (Table 3 and Figure 8), but as flow increases, α becomes larger (Table 3), indicating a decrease in the spatial variation of shear stress in relation to the mean.

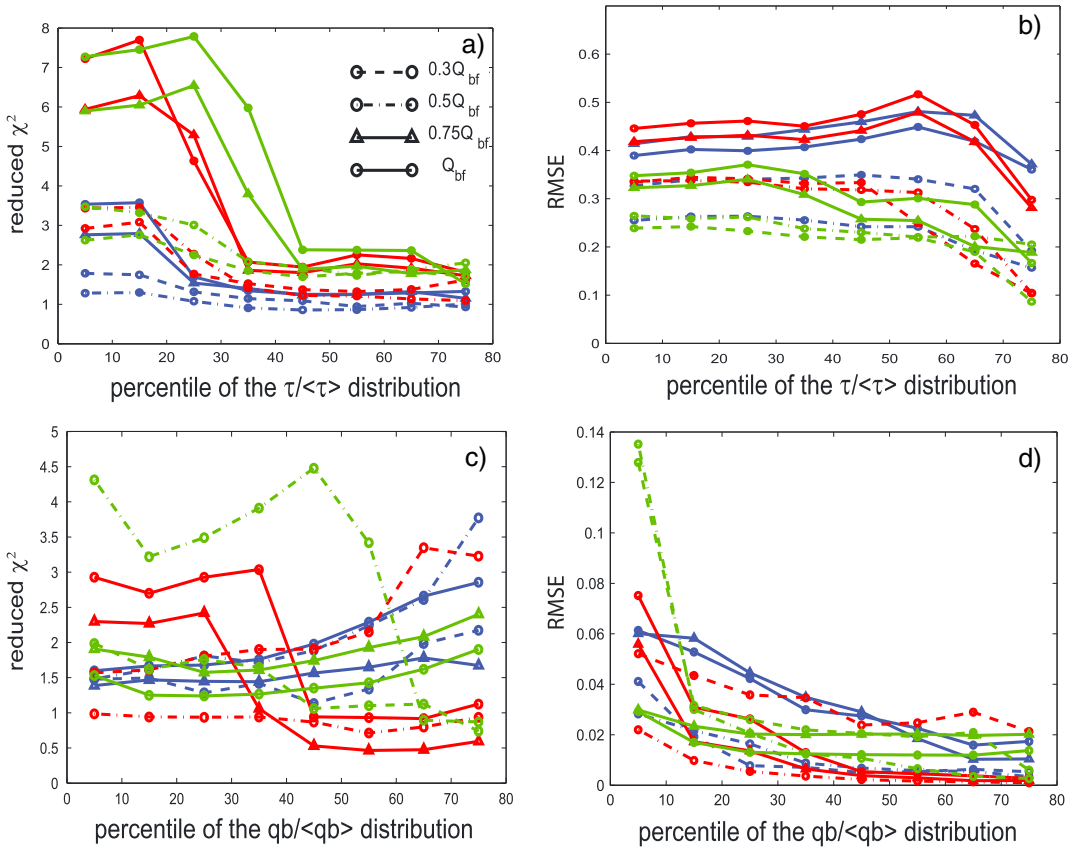

Figure 9. Partial reduced chi-square, χ^2_v, and Root mean square error, RMSE, of the gamma function fits to the mean-normalized distributions of shear stress, τ, and instantaneous unit-width bed load, q_b, for four flows at three sites. Both χ^2_v and RMSE are computed for subsets of each distribution including values above the 5th to 75th percentiles (i.e., excluding the lower values). The red markers and lines are for Site 1, blue for Site 2, and green for Site 3.

Even though the mean-normalized distributions of τ collapse to a single distribution, absolute values of τ vary greatly among sites. Both the mean and the range of τ values for the modeled flows are highest at Site 1, followed by Site 2, then Site 3 (Table 2); these differences are clearly related to downstream changes in slope. We also find that the mean shear stress estimated from the flow model, $\langle\tau\rangle$, is consistently lower than the reach-averaged shear stress obtained with (2) (Table 2). However, the difference between these two estimates of τ generally decreases with increasing flow, agreeing reasonably well as discharge approaches Q_{bf}. This is particularly the case for Sites 2 and 3, where the difference between the reach-averaged stress and mean-modeled stress is $<$13% (Table 2). The decreasing difference between the two estimates of τ with increasing discharge has to do with the fact that as flow increases, it becomes more uniform; consequently, the water surface slope is approximately the same as the friction slope. The difference in bankfull τ estimates at Site 1 is higher (19%) than at Sites 2 and 3 because this site is characterized by low relative submergence (ratio of depth to grain size). The general agreement between the reach-averaged shear stress and the model-derived mean shear stress suggests that observations of bankfull channel geometry (i.e., R) and water surface slope (S), together with the collapsed distributions of shear stress (Figure 7), can provide accurate estimates of the bankfull shear stress distribution at other locations in the watershed.

The percentage of the bed likely to be mobile for a given flow (i.e., percentage of grid cells with $\tau^*_{50} > \tau^*_{r,50}$) is consistently higher at Sites 1 and 3 than at Site 2 (Table 2). For instance, for the $0.3Q_{bf}$ flow the percentage of mobile bed area was 7.1 and 8.4 for Sites 1 and 3, respectively, and only 0.9 for Site 2 (Table 2). Maps of the ratio of $\tau^*_{50}/\tau^*_{c,50}$ at Q_{bf} indicate widespread mobility at Sites 1 and 3, with 54% and 65% of the channel beds experiencing $\tau^*_{50}/\tau^*_{c,50} > 1$ (Table 2 and Figure 10). In contrast, at Site 2 only one quarter of the channel experienced $\tau^*_{50}/\tau^*_{c,50} > 1$ at Q_{bf} (Figure 10 and Table 2). Complete mobilization of the bed reflecting stresses

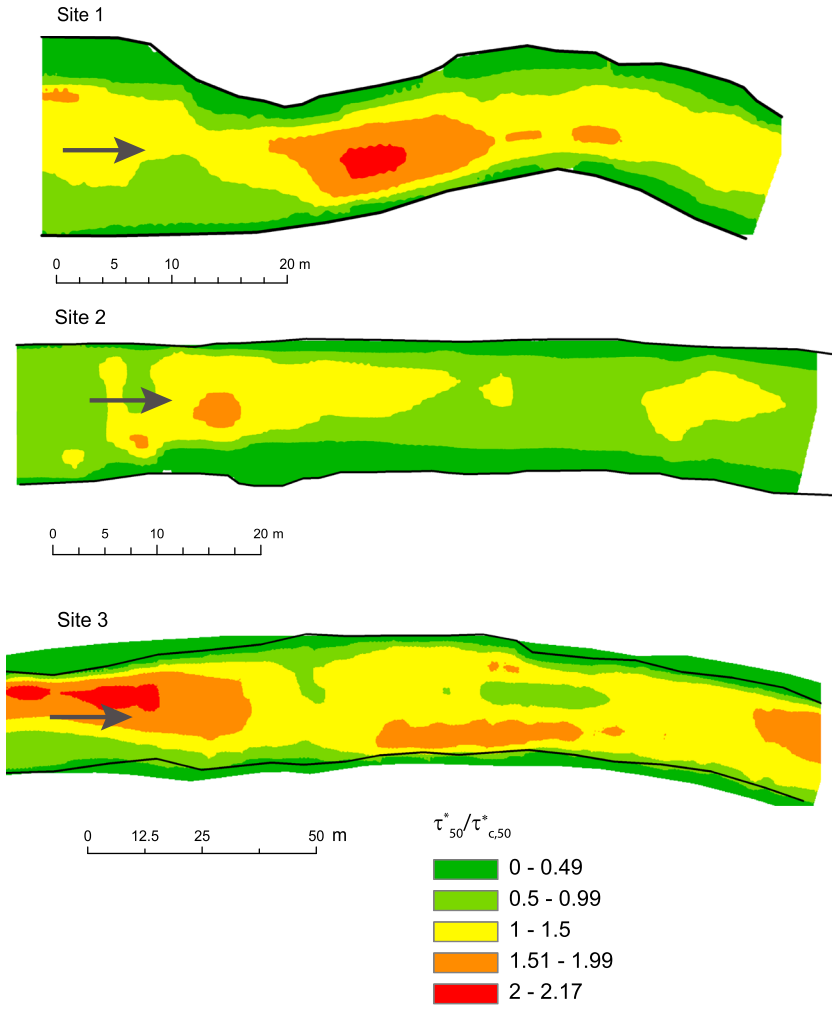

Figure 10. Spatial distribution of the ratio between available and critical Shields stress for the median grain size in the surface $\left(\tau^*_{50}/\tau^*_{c,50}\right)$ at bankfull flow at the study sites.

that are greater than roughly 2 times the threshold for motion [*Wilcock and McArdell*, 1993] is rare at any of the study sites; consequently, bed load movement is dominated by partial transport. We find that the shape parameter, α, of the gamma function that describes the τ distributions increases not only with discharge but also with transport stage, $\tau^*_{50}/\tau^*_{c,50}$ ($R^2 = 0.59$, $p = 0.0036$) which has also been reported by *Recking* [2013].

The rather stable conditions at Site 2 relative to Sites 1 and 3 are likely related to the fact that the surface grain size within this reach is large in comparison to the available shear stress. The median surface grain sizes of the channel at Sites 1 and 2 are statistically similar (t test, $p = 0.17$, Figure 3), whereas their median shear stress at Q_{bf} is statistically different (t test, $p \ll 0.00001$). The range in τ at Q_{bf} at Site 1 is more than twice the range observed for Site 2 (Table 2). Site 3, on the other hand, has similar levels of bed mobility at Q_{bf} to Site 1 because, even though the range of τ is lower than at Site 1 (Table 2), the grain size in this reach is significantly smaller (t test, $p < 0.00005$, Figure 3).

4.2. Variations in Instantaneous Transport Rates

The spatial distributions of unit-width bed load transport rates, q_b, (Figure 11) indicate that most of the load is transported through relatively small areas of the channel bed with high shear stresses (Figure 6). At the lowest modeled flow the proportion of the channel bed that is mobile varies between 18 and 6% at the three study sites (Table 3). These percentages increase as discharge increases, such that at Q_{bf} 87 to 51% of the bed is mobile (Table 3). At Q_{bf}, the unit-width transport rates, q_b, computed from (12) are 0.65, 0.035, and 0.17 kg/m/s

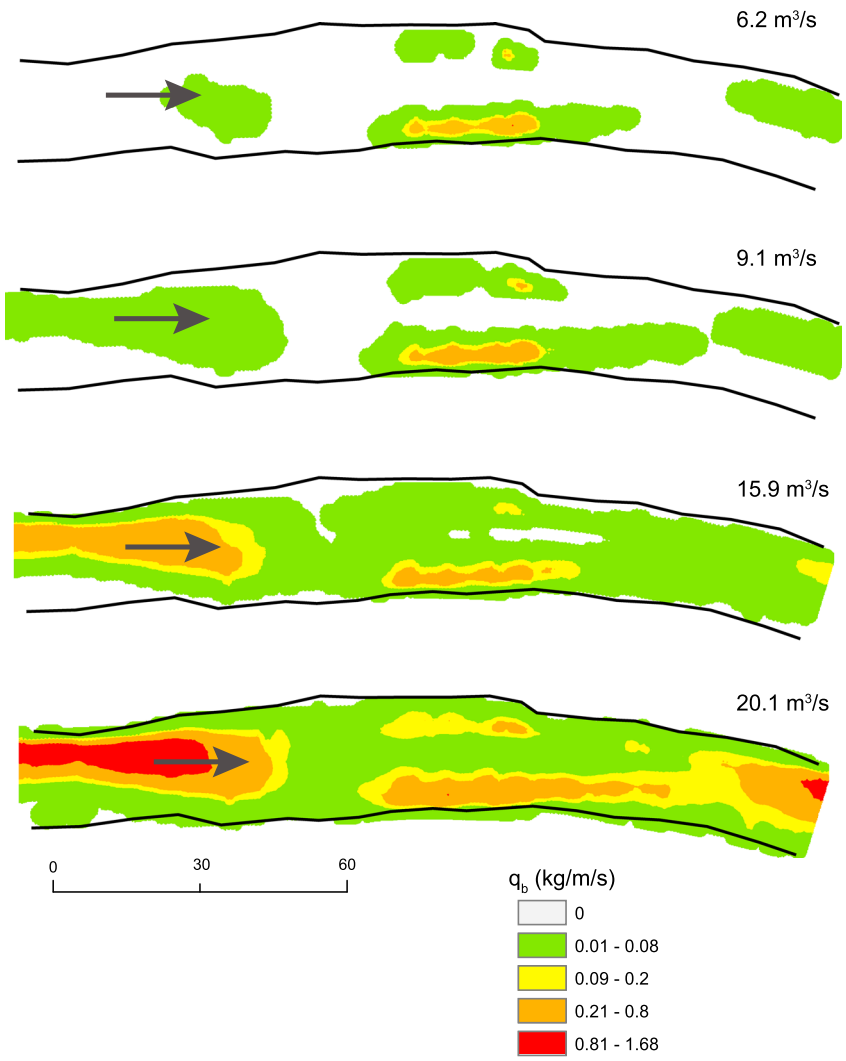

Figure 11. Modeled instantaneous unit-width transport rates (q_b) in kg/m/s in Site 3 for four flows. The areas colored white depicted locations in the bed in which the modeled shear stress is below the critical for motion for all subsurface grain size fractions.

at Sites 1, 2, and 3, respectively (Table 3). To assess whether these results are reasonable, we developed bed load rating curves for Sites 1 and 3 based on a series of flow and transport measurements taken at approximately the same locations, as reported by *Williams and Rosgen* [1989]. Bed load samples taken in conjunction with measurements of discharge, slope, and grain size allowed us develop empirical relations between discharge, shear stress, and bed load transport rate for a series of 16 flows at Site 1 and 19 flows at Site 3. Extrapolating these relations to bankfull discharge gives unit-width bed load transport rates of approximately 0.10 kg/m/s at the two USGS sites. The modeled transport rates bracket this value, with the high and low estimates (0.65 and 0.035 kg/m/s) spanning a little more than 1 order of magnitude. Measurements taken in the St. Louis Creek basin, ~12 km east of the Williams Fork, suggest that the maximum bed load transport rates at Q_{bf} are on the order of 0.010 kg/m/s [*Bunte et al.*, 2004], comparable to our estimate for Site 2, but much lower than our estimates for Sites 1 and 3. These discrepancies could be resolved by tuning the parameters of the transport model; however, our primary goal here is to present a simplified approach involving no more parameters than necessary to calculate bed load transport.

In contrast to the distributions of τ, the distributions of q_b are not symmetric, with most of the bed experiencing low transport rates at all four flows (Figure 7). The contrast between distributions is expressed in the significantly smaller shape parameter (α) of the gamma function for the q_b distributions

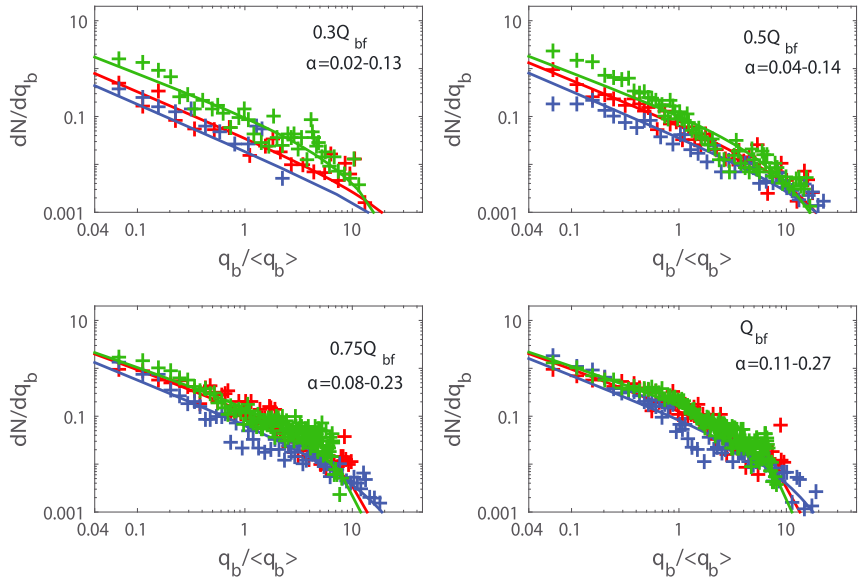

Figure 12. Frequency distributions of normalized instantaneous transport rate, q_b, at four discharge levels and three sites. The colored lines in each panel indicate the best fit to the gamma function. The red markers and lines are for Site 1, blue for Site 2, and green for Site 3.

compared to the τ distributions (Table 3 and Figure 12) and indicates that the degree of spatial variability is higher for the τ distributions relative to the q_b distributions. However, similar to the τ,the mean α value of the fit to the q_b distributions per flow level (i.e., mean α on each panel in Figure 12) increases with discharge ($R^2 = 0.61$, $p = 0.003$) and transport stage $\tau^*_{50}/\tau^*_{c,50}$ ($R^2 = 0.80$, $p = 0.0001$) and varied between 0.06 ± 0.06 for $0.3Q_{bf}$ and 0.19 ± 0.08 for Q_{bf} (Table 3), indicating that as discharge increases, the spatial variability also increases. From Figure 12 it is apparent that as discharge increases, the fitted gamma distributions are almost identical at all three sites (i.e., lines in Figure 12 for Q_{bf} are almost overlapping) indicating that when scaled by the reach average, the frequency distribution of instantaneous bed load transport rate is very similar at all three sites. The strength of the fits of the gamma function to the modeled q_b values is weaker than the fits to the τ distributions (Table 3). While the fits considering the complete distribution are weak (i.e., $\chi^2_v = 12$–52 and RMSE = 0.6–5, Table 3), partial fits considering q_b values above the 5th to the 75th percentiles of the distribution yield significantly stronger fits (Figure 9). For example, considering q_b values above the 5th percentile, the mean RMSE decreases from 1.9 to 0.05 highlighting the strength of the gamma function for modeling most of the distribution (Figure 9). This effect is not evident from the partial χ^2_v (Figure 9c) because the number of observations at high q_b intervals is small and thus the number of degrees of freedom is also small and varying between 4 and 133. This range is much smaller than for the τ distribution, for which the degrees of freedom are ~4 times larger (43–427).

The relative mobility of individual grain size fractions per flow and shear stress level was analyzed by computing Q_b (equation (12)) over individual grain size fractions (i). We found that as discharge increases, the grain size of the bed load becomes coarser (Figure 13). For Site 1, for example, the median grain size of the load ($D_{qb,50}$) increases from 5.3 to 25.8 mm between the smallest ($0.3Q_{bf}$) and largest modeled flow (Q_{bf}, Table 3). The bed load GSD closely resembles the subsurface at Q_{bf} for Sites 1 and 3 (Figure 13). The median grain size of the subsurface (D_{50s}) at the three sites varies between 10 and 24 mm (Table 3), whereas $D_{qb,50}$ varies between 1.5 and 26 mm at all sites for all flows (Table 3).

4.3. Basin-Wide Model of Bankfull Bed Load Transport

In this section we describe the extension of our results from three study sites to estimate bed load transport rates at other locations in the watershed. Our approach is based on the assumption that the shape of the mean-normalized distribution of bankfull shear stress is essentially the same across other sites in the basin, and thus, the local distribution of τ can be derived if the reach-averaged bankfull shear stress is known.

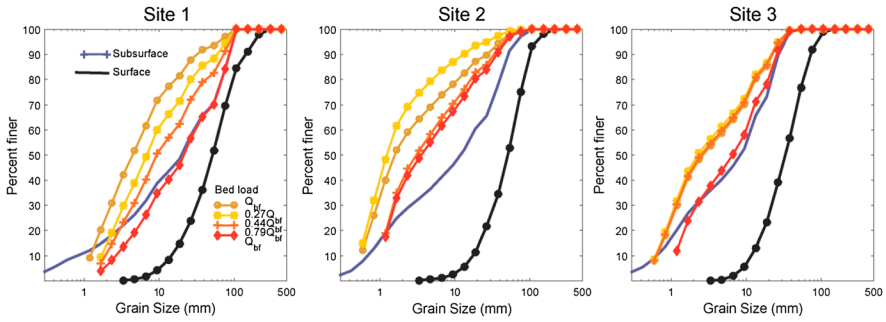

Figure 13. Grain size distributions, GSDs, of the field measured surface and subsurface and modeled bed load for four discharges and three sites.

Once this distribution is generated, it can be used together with measurements of the GSD distribution to compute the bankfull bed load transport rate. We tested this idea at 13 additional locations in the Williams Fork basin with drainage areas ranging between 14 and 387 km^2 (Figure 14). These additional locations are similar to the three study sites, meaning they are located in relatively straight alluvial reaches bordered by floodplains. For each of these locations we have measurements of bankfull channel geometry and surface and subsurface GSDs [*Pitlick et al*., 2008; *Segura*, 2008]. Based on these data, we first calculated the reach-averaged bankfull shear stress using (2) then scaled the collapsed distribution of shear stress (Figure 7) to obtain the local distribution of τ at Q_{bf}. We used the local distributions of shear stress, together with the measured subsurface GSD (Figure 3) and the transport relations ((8a) and (8b)), to compute bed load transport rates at Q_{bf}. The results of these calculations, shown in Figures 14b and 14c, suggest that when the estimates of q_b are normalized by the site mean and binned into appropriate intervals, the frequency distributions of transport rates collapse to a similar form. Fitting each of these distributions separately with the gamma function results in a mean shape parameter α of 0.19 ± 0.03 (Figure 14c), which is nearly identical to the mean value obtained for our three sites (0.19 ± 0.08). This similarity is not too surprising considering we used the same normalized distribution of τ across all sites; however, the site characteristics are sufficiently different that we might not expect the distributions of transport rates to be as similar as this analysis suggests.

5. Discussion

Two-dimensional flow modeling was used to describe the distributions of τ for discharge levels between $0.3Q_{bf}$ and Q_{bf} at three reaches of the Williams Fork River, CO. The results of the flow modeling indicate that these distributions for all flows and sites have the highest frequencies at intermediate values (Figure 7). However, at low flows the distributions are wider and right skewed for all sites. As flow increases, the mean-normalized τ distribution becomes narrower and approaches a symmetric function, with most of the observations concentrated around the median value. The shape of the τ distribution revealed similarities across sites for flow level considered. *Lisle et al*. [2000] observed a similar effect on the shape of the distribution of shear stress at Q_{bf} between small and large rivers in Colorado and California. They found that the distributions of τ are systematically wider for small channels than for large channels because large channels are less likely to be affected by large roughness elements relative to the flow depth. According to our results, the τ distributions are wider for low flows in which, analogous to *Lisle et al*. [2000], roughness elements are more likely to affect the flow structure. In addition to strong similarities in the τ distributions at Q_{bf}, we also found that the τ distributions for lower flows are also similar among sites. Thus, our findings suggest that it is possible to apply a simple scaling relation and assume a universal τ distribution per flow level transferable to anywhere in the watershed with similar channel morphology (e.g., relatively straight and well connected with the floodplain) where an estimate of the mean τ is available. We found that a reach-averaged estimate of shear stress (equation (2)) is very close to the mean and median modeled τ values for Q_{bf} (Table 2). The implications of these are important because it indicates the potential to scale the distribution of τ at Q_{bf} to different locations of a watershed based on flow modeling efforts on a small number of places and one-dimensional estimates of τ. The applicability of this methodology at low flows ($<0.5Q_{bf}$) has a higher level of uncertainty because there are higher

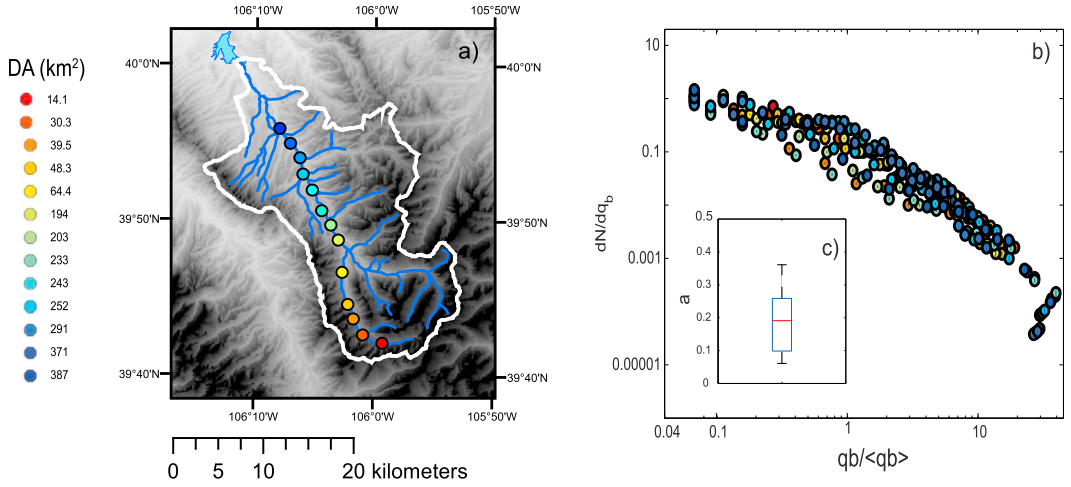

Figure 14. (a) Location and drainage area (DA) of 13 locations in the watershed where a basin-wide model to predict bed load was formulated. (b) Frequency distributions of normalized instantaneous transport rate, q_b, at Q_{bf} in all 13 locations. The color in the markers corresponds to the locations in Figure 14a. (c) Distribution of shape parameter α of the best fitted gamma function to q_b distributions in Figure 14b.

discrepancies (16–30%) between the median modeled τ and the uniform reach-averaged τ estimate. However, it is likely that these uncertainties would produce lower discrepancies between actual and estimated values of bed load than those attained using a one-dimensional approach (i.e., based on section average) which have been shown theoretically to underestimate bed load flux [*Paola*, 1996; *Nicholas*, 2000; *Ferguson*, 2003; *Bertoldi et al.*, 2009] and to both overestimate and underestimate the sediment flux by orders of magnitude when comparing observed and modeled values [*Rickenmann*, 2001; *Almedeij and Diplas*, 2003; *Barry et al.*, 2004; *Recking et al.*, 2012].

The shape of the τ distribution was parameterized using a gamma function, which parameters consistently increase with discharge in all sites (Table 3). Others have also used this function to model the distributions of τ and in some cases depth (H) in natural rivers [*Paola*, 1996; *Nicholas*, 2000, 2003; *Pitlick et al.*, 2012; *Recking*, 2013]. *Nicholas* [2000, 2003] used a gamma function to model the H and τ distributions and found that as discharge increases, the shape parameter, α, of both distributions also increases indicating lower degree of spatial variability in the distributions. This is a similar result to what we observed for α for both τ and q_b which in both cases increase with discharge. Also analogous to *Nicholas* [2000], we found that α for the τ distribution increases with stream size. In addition, the values of α per flow level were similar across sites indicating similar degrees of variability in the distribution. A direct comparison of specific α values between our study and *Nicholas* [2000, 2003] is not possible because he worked in braided rivers while our system is a single-threaded river. However, *Recking* [2013] argues that a value around 1.0 is typical of braided rivers while a value of around 5 would be typical of single-thread rivers. This is consistent with the mean overall value of 4.3 we found for our reaches. Finally, we also found a linear relation between transport stage $\left(\tau^*_{50}/\tau^*_{c,50}\right)$ and the α parameter of the τ distributions indicating that flow conditions are more variable at lower transport state. This relation has also been reported for braided rivers [*Recking*, 2013]. The $\tau^*_{50}/\tau^*_{c,50}$ ratios we found (between 0.31 and 1.05) are similar to previously reported values from gravel bed rivers [*Parker*, 1978; *Andrews*, 1983; *Ryan et al.*, 2002; *Mueller et al.*, 2005; *Parker et al.*, 2007] and are typical of partial mobility conditions even at Q_{bf} conditions.

Our second objective was to use the modeled estimates of shear stress along with measurements of the bed material grain size to describe the spatial (within the bed) and temporal (for different flow levels) variabilities of bed load transport per each reach. The spatial distributions of bed load transport rate indicated that large fractions of the channel bed, even at Q_{bf}, do not contribute to the sediment flux of grain sizes present in the subsurface. This is an important distinction relative to the spatial distributions of τ because even at very low flow (i.e., low depth or velocity), the flow exerts a force in the channel, by definition, above zero. These differences are evident by looking at the frequency distributions of flow H, τ, and q_b for Q_{bf} at Site 3

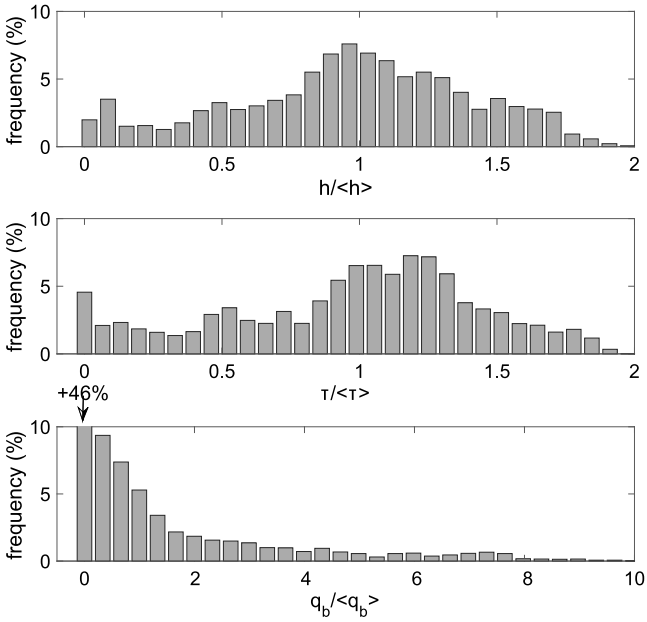

Figure 15. Comparison of the normalized frequency distributions of bankfull flow depth (H), shear stress (τ), and bed load transport (q_b) in Site 3.

(Figure 15). Both the distributions of H and τ are more or less symmetric with intermediate values having the largest frequencies in the channel bed and have a narrow range of values (i.e., less than twice the mean). Visual inspection indicates that the shape of the H distribution is similar to the shape reported by others [*Rosenfeld et al.*, 2011; *Legleiter*, 2014]. The distributions of q_b on the other hand are right skewed with the highest frequencies at the lowest values of transport. This distribution also indicates that while most locations in the channel experience very low transport rates, a very small fraction experiences up to 10 times the mean value. The level of skewness (and degree of variability) in the q_b distributions decreases with discharge and transport stage as expressed by the increases in the α parameter of the fitted gamma functions (Figure 12 and Table 3). However, these α values are ~6 times smaller than those found for H [*Pitlick et al.*, 2012] and between 20 and 150 times smaller than those found for τ for all flow levels and sites (Figure 8 and Table 3). Analogous to what we found for τ, the normalized distributions of q_b are similar among sites at Q_{bf} indicating that at this flow there is a balance between the GSD and the flow forces.

Our basin-wide model indicates that it is possible to generate distributions of Q_{bf} shear stress in other similar locations (i.e., similar sinuosity and connection to the floodplain) in the basin based only on reach-averaged shear stress values generated from channel geometry observations. Here we used these distributions together with subsurface GSD to compute unit-width bed load transport. However, there are other applications for these upscaling schemes. For instance, to model stream bed disturbance in the context of stream ecology, or can be used together with estimates of channel geometry and GSD [e.g., *Pitlick et al.*, 2008], to compute 2-D transport fluxes that would provide a first approximation of bed load transport rates at ungaged locations.

Despite the large variability in the spatial distribution of q_b, we found a smaller degree of variation in the GSD of the load. As others have found [*Parker et al.*, 1982; *Lisle*, 1995; *Clayton and Pitlick*, 2007; *Pitlick et al.*, 2008; *Lucia et al.*, 2013], the size of the load was finer than the surface and near in size to the subsurface for high flow levels. This was true for all sites indicating size selective processes of sediment transport of fine sediment or partial transport [*Ashworth and Ferguson*, 1989; *Lisle*, 1995; *Haschenburger and Wilcock*, 2003]. Full mobility does not characterize the transport mode of any of the discharges modeled in any site [*Wilcock and McArdell*, 1997]. At Q_{bf} the percentage of the bed with $\tau^* > 2\tau_c^*$ varies between 0 and 2% in all three sites. The ecological implications of this finding are important because it indicated that large grains are moved in a much smaller proportion than their abundance in the surface and therefore are probably important as refugia of benthic organisms during high flows. At Q_{bf} particles larger than 45 mm make up less than 20% of the load but are around 60% of the surface grain size in all sites (Figure 13).

6. Conclusions

In this paper a two-dimensional flow model in combination with surface and subsurface GSD information were used to study the spatial and temporal variations of τ and bed load transport in three alluvial gravel bed reaches and to build a basin-wide model to predict bed load transport. The results indicate that for all three sites the distributions of τ, at low flows ($<0.5\ Q_{bf}$), are right skewed, whereas at high flows (Q_{bf}) are

almost symmetric with most observations around the median value. These distributions are undistinguishable among sites when normalized by their mean value revealing statistically strong scaling properties and providing the basis for transferring reach-scale results to the entire watershed. The τ distributions were used in combination with subsurface GSD to compute bed load sediment transport. The distributions of unit-width instantaneous transport rates, q_b, for all flows are right skewed indicating that even at high flows (Q_{bf}) transport is limited to relatively small portions of the bed. We also found that the median grain size of the load consistently increases with discharge to resemble the distribution of the subsurface at Q_{bf}. We found that the normalized distributions of τ and q_b are well described by a gamma function especially for high τ and q_b values. The shape parameter of the gamma function increases with flow and transport stage in both cases. Based on the strong scaling properties of the distributions we generated a basin-wide sediment transport model. We assumed that the shape of the normalized distribution of τ in similar reaches in the basin is identical to the mean distribution observed at the three study sites. This *universal* mean-normalized shape was used in combination with reach-averaged bankfull τ at 13 additional sites to infer their nonnormalized τ distribution. These distributions together with site-specific subsurface GSD observations were used to derive the corresponding q_b distributions. We found that these distributions are similar among sites highlighting a basin-wide balance between flow forces and GSD. We believe that our results are a step forward toward the formulation of a basin-wide model of bed load transport. Further refinements to the model could be achieved by incorporating modeling efforts in other reaches, by conducting interbasin comparisons, by comparing measured and modeled transport rates, and by incorporating the flow frequency distribution of model flows to estimate annual bed load transport rates.

Acknowledgments

The data for this paper are available upon request to Catalina Segura at Catalina.segura@oregonstate.edu. Portions of this work have been funded by grants from the National Science Foundation (BCS-9986338) and the U.S. Forest Service (03-CS-11221625-122). Richard McDonald of the USGS provided very useful suggestions in the hydrodynamic model MD-SWMS. We also thank Laura MacGregor, Brandy Logan, and Kristina Wynne for all their help collecting field data. Finally, we would like to thank the Editor, Alex Densmore, Associate Editor, Amy Draught East, and three anonymous reviewers for providing very helpful, detailed comments on an earlier version of this manuscript.

References

Almedeij, J. H., and P. Diplas (2003), Bedload transport in gravel-bed streams with unimodal sediment, *J. Hydraul. Eng.*, *129*(11), 896–904, doi:10.1061/(asce)0733-9429(2003)129:11(896).

Andrews, E. D. (1983), Entrainment of gravel from naturally sorted riverbed material, *Geol. Soc. Am. Bull.*, *94*(10), 1225–1231, doi:10.1130/0016-7606(1983)94<1225:eogfns>2.0.co;2.

Asahi, K., Y. Shimizu, J. Nelson, and G. Parker (2013), Numerical simulation of river meandering with self-evolving banks, *J. Geophys. Res. Earth Surf.*, *118*, 2208–2229, doi:10.1002/jgrf.20150.

Ashworth, P. J., and R. I. Ferguson (1989), Size-selective entrainment of bed-load in gravel bed streams, *Water Resour. Res.*, *25*(4), 627–634, doi:10.1029/WR025i004p00627.

Bagnold, R. A. (1966), Shearing and dilatation of dry sand and singing mechanism, *Proc. R. Soc. London, Ser. A*, *295*(1442), 219–232, doi:10.1098/rspa.1966.0236.

Barry, J. J., J. M. Buffington, and J. G. King (2004), A general power equation for predicting bed load transport rates in gravel bed rivers, *Water Resour. Res.*, *40*, W10401, doi:10.1029/2004WR003190.

Bertoldi, W., P. Ashmore, and M. Tubino (2009), A method for estimating the mean bed load flux in braided rivers, *Geomorphology*, *103*(3), 330–340.

Bevington, P. R., and D. K. Robinson (2003), *Data Reduction and Error Analysis for the Physical Sciences*, 320 pp., McGraw-Hill, Boston, Mass.

Bunte, K., S. R. Abt, J. P. Potyondy, and S. E. Ryan (2004), Measurement of coarse gravel and cobble transport using portable bedload traps, *J. Hydraul. Eng.*, *130*(9), 879–893, doi:10.1061/(asce)0733-9429(2004)130:9(879).

Church, M., and M. A. Hassan (1992), Size and distance of travel of unconstrained clasts on a streambed, *Water Resour. Res.*, *28*(1), 299–303, doi:10.1029/91WR02523.

Church, M., D. G. McLean, and J. F. Walcott (1987), River bed gravels: Sampling and analysis, in *Sediment Transport in Gravel-Bed Rivers*, edited by C. R. Thorne, J. C. Bathurst, and R. D. Hey, pp. 43–88, John Wiley, Chichester, U. K.

Cienciala, P., and M. A. Hassan (2013), Linking spatial patterns of bed surface texture, bed mobility, and channel hydraulics in a mountain stream to potential spawning substrate for small resident trout, *Geomorphology*, *197*, 96–107.

Clayton, J. A., and J. Pitlick (2007), Spatial and temporal variations in bed load transport intensity in a gravel bed river bend, *Water Resour. Res.*, *43*, W02426, doi:10.1029/2006WR005253.

Dietrich, W. E. (1982), Settling velocity of natural particles, *Water Resour. Res.*, *18*(6), 1615–1626, doi:10.1029/WR018i006p01615.

Eke, E. C., M. J. Czapiga, E. Viparelli, Y. Shimizu, J. Imran, T. Sun, and G. Parker (2014), Coevolution of width and sinuosity in meandering rivers, *J. Fluid Mech.*, *760*, 127–174, doi:10.1017/jfm.2014.556.

Emmett, W. W. (1980), A field calibration of the sediment-trapping characteristics of the Helley-Smith bedload sampler, *U.S. Geol. Surv. Prof. Pap.*, *1139*, 41.

Engelund, F. (1974), Flow and bed topography in channel bends, *J. Hydraul. Div., Am. Soc. Civ. Eng.*, *100*(11), 1631–1648.

Ferguson, R. I. (2003), The missing dimension: Effects of lateral variation on 1-D calculations of fluvial bedload transport, *Geomorphology*, *56*(1–2), 1–14, doi:10.1016/s0169-555x(03)00042-4.

Ferguson, R. I., and S. J. Wathen (1998), Tracer-pebble movement along a concave river profile: Virtual velocity in relation to grain size and shear stress, *Water Resour. Res.*, *34*(8), 2031–2038, doi:10.1029/98WR01283.

Ferguson, R. I., D. R. Parsons, S. N. Lane, and R. J. Hardy (2003), Flow in meander bends with recirculation at the inner bank, *Water Resour. Res.*, *39*(11), 1322, doi:10.1029/2003WR001965.

Habersack, H. M., and J. B. Laronne (2001), Bed load texture in an alpine gravel bed river, *Water Resour. Res.*, *37*(12), 3359–3370, doi:10.1029/2001WR000260.

Harrison, L. R., C. J. Legleiter, M. A. Wydzga, and T. Dunne (2011), Channel dynamics and habitat development in a meandering, gravel bed river, *Water Resour. Res.*, *47*, W04513, doi:10.1029/2009WR008926.

Haschenburger, J. K. (1999), A probability model of scour and fill depths in gravel-bed channels, *Water Resour. Res.*, *35*(9), 2857–2869, doi:10.1029/1999WR900153.
Haschenburger, J. K., and P. R. Wilcock (2003), Partial transport in a natural gravel bed channel, *Water Resour. Res.*, *39*(1), 1020, doi:10.1029/2002WR001532.
Hassan, M. A., and M. Church (2001), Sensitivity of bed load transport in Harris Creek: Seasonal and spatial variation over a cobble-gravel bar, *Water Resour. Res.*, *37*(3), 813–825, doi:10.1029/2000WR900346.
Kellogg, K. S. (2001), Tectonic controls on a large landslide complex: Williams Fork Mountains near Dillon, Colorado, *Geomorphology*, *41*(4), 355–368, doi:10.1016/S0169-555X(01)00067-8.
Kinzel, P. J., J. M. Nelson, and A. K. Heckman (2009), Respones of sandhill crane (Grus canadensis) riverine roosting habitat to changes in stage and sandbar morphology, *River Res. Appl.*, *25*(2), 135–152, doi:10.1002/rra.1103.
Lane, S. N., K. F. Bradbrook, K. S. Richards, P. A. Biron, and A. G. Roy (1999), The application of computational fluid dynamics to natural river channels: Three-dimensional versus two-dimensional approaches, *Geomorphology*, *29*(1–2), 1–20, doi:10.1016/S0169-555X(99)00003-3.
Legleiter, C. J. (2014), A geostatistical framework for quantifying the reach-scale spatial structure of river morphology: 1. Variogram models, related metrics, and relation to channel form, *Geomorphology*, *205*, 65–84, doi:10.1016/j.geomorph.2012.01.016.
Legleiter, C. J., P. C. Kyriakidis, R. R. McDonald, and J. M. Nelson (2011), Effects of uncertain topographic input data on two-dimensional flow modeling in a gravel-bed river, *Water Resour. Res.*, *47*, W03518, doi:10.1029/2010WR009618.
Lisle, T. E. (1995), Particle-size variations between bed-load and bed material in natural gravel-bed channels, *Water Resour. Res.*, *31*(4), 1107–1118, doi:10.1029/94WR02526.
Lisle, T. E., J. M. Nelson, J. Pitlick, M. A. Madej, and B. L. Barkett (2000), Variability of bed mobility in natural, gravel-bed channels and adjustments to sediment load at local and reach scales, *Water Resour. Res.*, *36*(12), 3743–3755, doi:10.1029/2000WR900238.
Logan, B. L., R. R. McDonald, J. M. Nelson, P. J. Kinzel, and G. J. Barton (2011), Use of multidimensional modeling to evaluate a channel restoration design for the Kootenai River, Idaho, 68 pp.
Lucia, A., A. Recking, J. F. Martin-Duque, Y. Storz-Peretz, and J. B. Laronne (2013), Continuous monitoring of bedload discharge in a small, steep sandy channel, *J. Hydrol.*, *497*, 37–50, doi:10.1016/j.jhydrol.2013.05.034.
May, C. L., B. Pryor, T. E. Lisle, and M. Lang (2009), Coupling hydrodynamic modeling and empirical measures of bed mobility to predict the risk of scour and fill of salmon redds in a large regulated river, *Water Resour. Res.*, *45*, W05402, doi:10.1029/2007WR006498.
McDonald, R. R., J. P. Bennett, and J. M. Nelson (2001), The USGS multi-dimensional surface water modeling system, paper presented at 7th Proceedings of the Federal Interagency Sedimentation Conference, Subcommittee on Sedimentation, Reno, Nev., 21–25 March.
McDonald, R. R., J. M. Nelson, P. J. Kinzel, and J. S. Conaway (2006), Modeling surface-water flow and sediment mobility with the multi-dimensional surface water modeling system (MD_SWMS), *U.S. Geol. Surv. Sci. Invest. Rep.*, 6 pp.
McDonald, R. R., J. Nelson, V. Paragamian, and G. Barton (2010), Modeling the effect of flow and sediment transport on White Sturgeon spawning habitat in the Kootenai River, Idaho, *J. Hydraul. Eng.*, *136*(12), 1077–1092, doi:10.1061/(ASCE)HY.1943-7900.0000283.
McKean, J., and D. Tonina (2013), Bed stability in unconfined gravel bed mountain streams: With implications for salmon spawning viability in future climates, *J. Geophys. Res. Earth Surf.*, *118*, 1227–1240, doi:10.1002/jgrf.20092.
Mosselman, E. (1998), Morphological modelling of rivers with erodible banks, *Hydrol. Processes*, *12*(8), 1357–1370, doi:10.1002/(sici)1099-1085(19980630)12:8<1357::aid-hyp619>3.3.co;2-z.
Mueller, E. R., J. Pitlick, and J. M. Nelson (2005), Variation in the reference Shields stress for bed load transport in gravel-bed streams and rivers, *Water Resour. Res.*, *41*, W04006, doi:10.1029/2004WR003692.
Nelson, J. M. (1990), The initial instability and finite-amplitude stability of alternate bars in straight channels, *Earth Sci. Rev.*, *29*(1–4), 97–115, doi:10.1016/0012-8252(0)90030-y.
Nelson, J. M., and J. D. Smith (1989), Flow in meandering channels with natural topography, in *River Meandering*, *Water Resour. Monogr.*, vol. 12, edited by S. Ikeda and G. Parker, pp. 69–102, AGU, Washington, D. C.
Nelson, J. M., J. P. Bennett, and S. Wiele (2003), Flow and sediment transport modeling, in *Tools in Fluvial Geomorphology*, edited by G. M. Kondolph and H. Piegay, chap. 18, pp. 539–576, Wiley, Chichester, U. K.
Nelson, J. M., B. L. Logan, P. J. Kinzel, Y. Shimizu, S. Giri, R. L. Shreve, and S. R. McLean (2011), Bedform response to flow variability, *Earth Surf. Processes Landforms*, *36*(14), 1938–1947, doi:10.1002/Esp.2212.
Nelson, P. A., W. E. Dietrich, and J. G. Venditti (2010), Bed topography and the development of forced bed surface patches, *J. Geophys. Res.*, *115*, F04024, doi:10.1029/2010JF001747.
Newman, M. E. J. (2005), Power laws, Pareto distributions and Zipf's law, *Contemp. Phys.*, *46*(5), 323–351, doi:10.1080/00107510500052444.
Nicholas, A. P. (2000), Modelling bedload yield in braided gravel bed rivers, *Geomorphology*, *36*(1–2), 89–106, doi:10.1016/S0169-555X(00)00050-7.
Nicholas, A. P. (2003), Investigation of spatially distributed braided river flows using a two-dimensional hydraulic model, *Earth Surf. Processes Landforms*, *28*(6), 655–674, doi:10.1002/esp.491.
Paola, C. (1996), Incoherent structures: Turbulence as a metaphor for stream braiding, in *Coherent Flow Structures in Open Channels*, edited by P. J. Ashworth et al., pp. 706–723, John Wiley, Chichester, U. K.
Papanicolaou, A. N., M. Elhakeem, D. Dermisis, and N. Young (2011), Evaluation of the Missouri River shallow water habitat using a 2D-hydrodynamic model, *River Res. Appl.*, *27*(2), 157–167, doi:10.1002/rra.1344.
Parker, G. (1978), Self-formed straight rivers with equilibrium banks and mobile bed: Part 2. The gravel river, *J. Fluid Mech.*, *89*, 127.
Parker, G. (1979), Hydraulic geometry of active gravel rivers, *J. Hydraul. Div., Am. Soc. Civ. Eng.*, *105*, 1185–1201.
Parker, G. (1990), Surface-based bedload transport relation for gravel rivers, *J. Hydraul. Res.*, *28*, 417–436.
Parker, G., and E. D. Andrews (1985), Sorting of bed load sediment by flow in meander bends, *Water Resour. Res.*, *21*(9), 1361–1373, doi:10.1029/WR021i009p01361.
Parker, G., and P. C. Klingeman (1982), On why gravel bed streams are paved, *Water Resour. Res.*, *18*(5), 1409–1423, doi:10.1029/WR018i005p01409.
Parker, G., P. C. Klingeman, and D. G. McLean (1982), Bedload and size distribution in paved gravel-bed streams, *J. Hydraul. Div., Am. Soc. Civ. Eng.*, *108*, 544–571.
Parker, G., P. R. Wilcock, C. Paola, W. E. Dietrich, and J. Pitlick (2007), Physical basis for quasi-universal relations describing bankfull hydraulic geometry of single-thread gravel bed rivers, *J. Geophys. Res.*, *112*, F04005, doi:10.1029/2006JF000549.
Pasternack, G. B., C. L. Wang, and J. E. Merz (2004), Application of a 2D hydrodynamic model to design of reach-scale spawning gravel replenishment on the Mokelumne River, California, *River Res. Appl.*, *20*(2), 205–225, doi:10.1002/rra.748.
Pitlick, J. (1988), Variability of bed load measurement, *Water Resour. Res.*, *24*(1), 173–177, doi:10.1029/WR024i001p00173.

Pitlick, J., E. R. Mueller, C. Segura, R. Cress, and M. Torizzo (2008), Relation between flow, surface-layer armoring and sediment transport in gravel-bed rivers, *Earth Surf. Processes Landforms*, *33*(8), 1192–1209, doi:10.1002/esp.1607.

Pitlick, J., E. R. Mueller, and C. Segura (2012), Differences in sediment supply to braided and single-thread river channels: What do the data tell us?, in *Gravel Bed Rivers: Processes, Tools, Environments*, edited by M. A. Church, P. Brion, and A. H. Roy, pp. 502–511, Wiley, Chichester, U. K.

Press, W. H., S. A. Teukolsky, W. T. Vetterling, and B. P. Flannery (2007), *Numerical Recipes: The Art of Scientific Computing*, 1235 pp., Cambridge Univ. Press, New York.

Pyrce, R. S., and P. E. Ashmore (2003), Particle path length distributions in meandering gravel-bed streams: Results from physical models, *Earth Surf. Processes Landforms*, *28*(9), 951–966, doi:10.1002/esp.498.

Recking, A. (2010), A comparison between flume and field bed load transport data and consequences for surface-based bed load transport prediction, *Water Resour. Res.*, *46*, W03518, doi:10.1029/2009WR008007.

Recking, A. (2013), An analysis of nonlinearity effects on bed load transport prediction, *J. Geophys. Res. Earth Surf.*, *118*, 1264–1281, doi:10.1002/jgrf.20090.

Recking, A., F. Liebault, C. Peteuil, and T. Jolimet (2012), Testing bedload transport equations with consideration of time scales, *Earth Surf. Processes Landforms*, *37*(7), 774–789, doi:10.1002/esp.3213.

Rickenmann, D. (2001), Comparison of bed load transport in torrents and gravel bed streams, *Water Resour. Res.*, *37*(12), 3295–3305, doi:10.1029/2001WR000319.

Rosenfeld, J. S., K. Campbell, E. S. Leung, J. Bernhardt, and J. Post (2011), Habitat effects on depth and velocity frequency distributions: Implications for modeling hydraulic variation and fish habitat suitability in streams, *Geomorphology*, *130*(3–4), 127–135, doi:10.1016/j.geomorph.2011.03.007.

Ryan, S. E., L. S. Porth, and C. A. Troendle (2002), Defining phases of bedload transport using piecewise regression, *Earth Surf. Processes Landforms*, *27*(9), 971–990, doi:10.1002/esp.387.

Segura, C. (2008), *Effects of Sediment Transport on Benthic Organisms in a Mountain River, CO*, 191 pp., Univ. of Colorado, Boulder, Colo.

Segura, C., and J. Pitlick (2010), Scaling frequency of channel-forming flows in snowmelt-dominated streams, *Water Resour. Res.*, *46*, W06524, doi:10.1029/2009WR008336.

Segura, C., J. H. McCutchan, W. M. Lewis Jr., and J. Pitlick (2011), The influence of channel bed disturbance on algal biomass in a Colorado mountain stream, *Ecohydrology*, *4*(3), 411–421, doi:10.1002/eco.142.

Serreze, M. C., M. P. Clark, R. L. Armstrong, D. A. McGinnis, and R. S. Pulwarty (1999), Characteristics of the western United States snowpack from snowpack telemetry (SNOTEL) data, *Water Resour. Res.*, *35*(7), 2145–2160, doi:10.1029/1999WR900090.

Shafroth, P. B., A. C. Wilcox, D. A. Lytle, J. T. Hickey, D. C. Andersen, V. B. Beauchamp, A. Hautzinger, L. E. McMullen, and A. Warner (2010), Ecosystem effects of environmental flows: Modelling and experimental floods in a dryland river, *Freshwater Biol.*, *55*(1), 68–85, doi:10.1111/j.1365-2427.2009.02271.x.

Sloff, K., and E. Mosselman (2012), Bifurcation modelling in a meandering gravel-sand bed river, *Earth Surf. Processes Landforms*, *37*(14), 1556–1566, doi:10.1002/esp.3305.

Stewart, G., R. Anderson, and E. Wohl (2005), Two-dimensional modelling of habitat suitability as a function of discharge on two Colorado rivers, *River Res. Appl.*, *21*(10), 1061–1074, doi:10.1002/rra.868.

Torizzo, M., and J. Pitlick (2004), Magnitude-frequency of bed load transport in mountain streams in Colorado, *J. Hydrol.*, *290*(1–2), 137–151, doi:10.1016/j.jhydrol.2003.12.001.

Tweto, O., and J. C. Reed (1973), Reconnaissance geologic map of the Ute Peak 15-minute Quadrangle, Grand and Summit counties, Colorado, Open Report 73-288, USGS.

Wathen, S. J., R. I. Ferguson, T. B. Hoey, and A. Werritty (1995), Unequal mobility of gravel and sand in weakly bimodal river sediments, *Water Resour. Res.*, *31*(8), 2087–2096, doi:10.1029/95WR01229.

Whiting, P. J., and W. E. Dietrich (1991), Convective accelerations and boundary shear-stress over a channel bar, *Water Resour. Res.*, *27*(5), 783–796, doi:10.1029/91WR00083.

Wilcock, P. R. (1988), Methods for estimating the critical shear-stress of individual fractions in mixed-size sediment, *Water Resour. Res.*, *24*(7), 1127–1135, doi:10.1029/WR024i007p01127.

Wilcock, P. R. (2001), Toward a practical method for estimating sediment-transport rates in gravel-bed rivers, *Earth Surf. Processes Landforms*, *26*, 1395–1408.

Wilcock, P. R., and B. W. McArdell (1993), Surface-based fractional transport rates: Mobilization thresholds and partial transport of a sand-gravel sediment, *Water Resour. Res.*, *29*(4), 1297–1312, doi:10.1029/92WR02748.

Wilcock, P. R., and B. W. McArdell (1997), Partial transport of a sand/gravel sediment, *Water Resour. Res.*, *33*(1), 235–245, doi:10.1029/96WR02672.

Williams, G. P., and D. L. Rosgen (1989), *Measure Total Sediment Loads (Suspended Loads and Bedloads)*, Rep. 89-67, U.S. Geol. Surv., Denver, Colo.

Williams, R. D., J. Brasington, M. Hicks, R. Measures, C. D. Rennie, and D. Vericat (2013), Hydraulic validation of two-dimensional simulations of braided river flow with spatially continuous aDcp data, *Water Resour. Res.*, *49*, 5183–5205, doi:10.1002/wrcr.20391.

Yager, E. M., W. E. Dietrich, J. W. Kirchner, and B. W. McArdell (2012), Patch dynamics and stability in steep, rough streams, *J. Geophys. Res.*, *117*, F02010, doi:10.1029/2011JF002253.